University of Alberta

Sustained Drug Release And Antibacterial Activity Of Ampicillin
incorporated Poly (methyl methacrylate)-Nylon6 Core/Shell Nanofibers

by

Amirreza Sohrabi

A thesis is submitted to the Faculty of Graduate Studies and Research in partial
fulfillment of the requirements for the degree of

Master of Science

In

Materials Engineering

Department of the Chemical and Materials Engineering

Dedication

I would like to dedicate this thesis to my great family whose support and encouragement has always enlightened my life and my wife whose helps made this study possible.

Abstract

A drug delivery system was designed based on the encapsulation of Ampicillin sodium salt in Poly (methyl methacrylate)(PMMA)-Nylon6 core/shell nanofibers and the release characteristics and antibacterial activity of the system were investigated. It was revealed that the system is capable of releasing the drug with a sustained manner through a three stages release in which the release in stage I followed the non-Fickian diffusion; however, Fickian diffusion was proven to be the release mechanism of stages II and III. The diffusion coefficient calculations indicated a significant decrease in the coefficient from stage II to stage III which is believed to be the consequent of fibers crystallization as a result of the long-term incubation in an aqueous solution. Finally, the antibacterial activity of the system was verified by means of optical density (OD) measurements against gram positive *L.innocua.*

Acknowledgement

Table of contents

List of tables

List of figures

List of abbreviations

°C	Degree centigrade
1D	One dimensional
3D	Three dimensional
Ac	Alternating current
AC	Ampicillin sodium salt
APT	All-purpose tween
BMP-2	Bone morphogenetic protein 2
BSA	Bovine serum albumin
cm	Centimeter
Cr	Chromium
CWP	Clean water permeability
Dc	Direct current
E	Electric field
E.coli	Escherichia coli
ECM	Extra cellular matrix
Eq.	Equation
FCS	Fluorescence correlation spectroscopy
Fig.	Figure
g	Gram
HCl	Hydrogen chloride
hr	Hour
ID	Inner diameter
kV	Kilovolt
M	Molar
mA	Milliamp
MBR	Membrane bioreactor
min	Minute
ml	Milliliter
mm	millimeter
N_2	Nitrogen gas
NF	nanofiber
NF-AC	Ampicillin encapsulated in nanofibers
NH_3	Ammonia
nHAP	Hydroxyapatite nanoparticle
Ni	Nickel
nm	Nanometer
OD	Outer diameter
OD	Optical density

PAA	Poly (acrylic acid)
PBS	Potassium buffer solution
PCL	Poly (caprolactone)
PEG	Poly (ethylene glycol)
PEO	Poly (ethylene oxide)
PEO-b-PCL	Poly (ethylene oxide)-b-poly (caprolactone)
PET	Poly (ethylene terephthalate)
PLA	Poly (lactic acid)
PLGA	Poly (lactide-co-glycolide)
PLLA	Poly (L-lactic acid)
PLLA/HA	Poly (L-lactide)-hydroxyapatite
PMMA	Poly (methyl methacrylate)
PP	Poly (propylene)
ppm	Parts per million
PS	Poly (styrene)
PU	Poly (urethane)
PVA	Poly (vinyl alcohol)
QCM	Quartz crystal microbalance
s	Second
SEM	Scanning electron microscopy
TEM	Transmission electron microscopy
UV-Vis spectroscopy	Ultraviolet-Visible spectroscopy
V	Volt
v/v	Volume to volume ratio
wt%	Weight percentage
ZnO	Zinc oxide
μg	Microgram

Chapter 1: Introduction

In this chapter, a brief introduction to electrospinning including the background of electrospinning and its basic concepts is delivered. Afterwards, different applications of electrospinning with the focus on the drug delivery application is discussed.

1.1. Background of electrospinning

Electrospinning is a very well-known technique amongst all fiber fabrication methods which share the characterizations of both electrospraying and conventional solution dry spinning [1]. The initial basics of the electrospinning came to life in 1745 when Bose investigated the formation of aerosols by applying high electric potentials to droplets of a fluid [2]. Almost a century later, in 1882, Lord Rayleigh investigated one of the most important aspects of electrospinning, namely the number of charges required to overcome the surface tension of a liquid droplet [3]. A few years later, the first device which was able to spray liquids with the application of a high electric potential was patented by Cooley and Morton in 1902 and 1903 [4-6]. Later, the fabrication of artificial silk through the application of a high voltage and the electrospinning of the plastic for the first time were performed by Hagiwaba et al. and Formhals [7,8]. In spite of numerous advancements in the area of electrospinning in that era, its application in industry had not been established yet. The electrospun fibers are believed to gain their first application as commercial products in nonwovens industry as filters [9].

In 1990's, Reneker group introduced the electrospinning to academia which established a new era of research in electrospinning [10]. One of the most important reasons that electrospinning has attracted the attention of many researchers from different disciplines of science and engineering is that it represents the combination of the fundamental as well as application-oriented research. These studies usually share the target of producing complex and highly functional systems with high commercial potential [11].

1.2. Concepts of electrospinning

The process of electrospinning involves applying a high electric field between a polymer droplet at a metal nozzle and a plate shaped counter electrode placed at a distance. The simple concept of electrospinning has rendered this technique as a useful method to fabricate fibers in the range of microns to a few nanometers with various potential applications [12]. Fig. 1-1 illustrates the schematic of an electrospinning setup utilized to fabricate electrospun fibers.
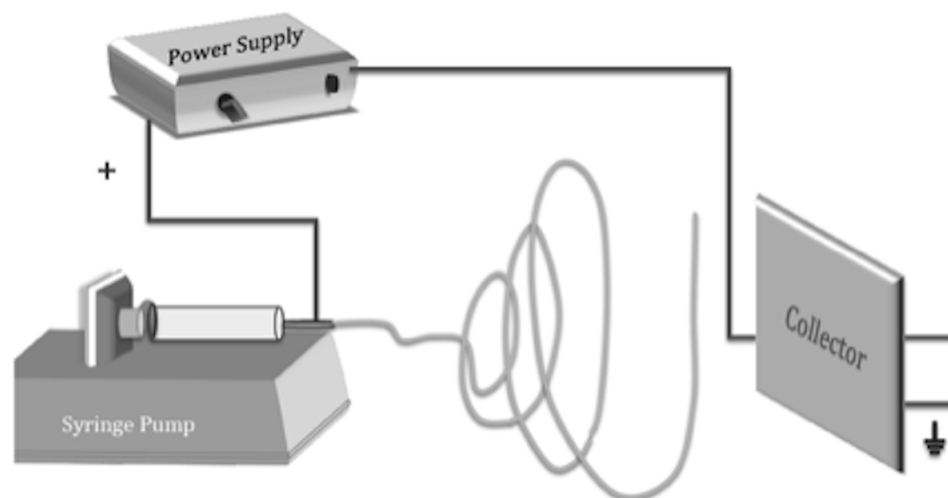
Fig. 1-1. Schematic of the elctrospinning apparatus.

The general procedure which could be observed in any electrospinning process is the application of a high voltage to the metallic nozzle and the deformation of the droplet to form a cone, known as the Taylor cone as illustrated
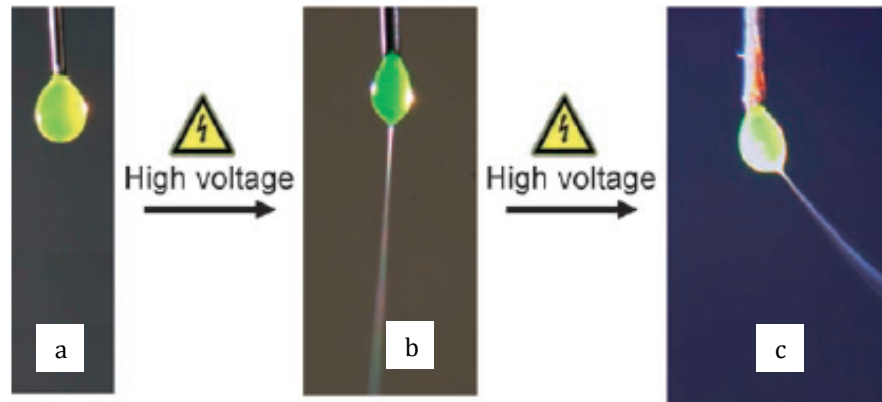
Fig. 1-2. The formation of the Taylor cone as a consequence of a high voltage for a 5% solution of Poly (ethylene oxide)(PEO) a) In the absence of high voltage b) At the applied voltage of 20kV with the jet perpendicular to the collector c) At the applied voltage of 20kV with the jet diagonal to the collector [11].

in

Fig. 1-2. If the applied voltage reaches a threshold amount in which the surface tension of the polymeric droplet could be overcome by the electrostatic forces, a jet will be formed which is accelerated towards the grounded collector [13-16]. The detailed process which a jet undergoes will be discussed in section 2.1.

1.3. Types of electrospinning

Generally, electrospinning could be performed on polymeric solutions as well as molten polymers. Basically, in the solution-based electrospinning, a solution of a polymer is used as the electrospinning solution. On the other hand, in the molten-based electrospinning technique, a polymer is melted and could be used for electrospinning without the application of any solvent. Many advantages and disadvantages are associated with each of these methods. The most important

advantage of the solution-based electrospinning is its ability to produce fine fibers in the range of a few nanometers by the judicial choice of spinning parameters. However, the solvent utilized to prepare the solution should evaporate during the electrospinning process to form the fibers. This evaporation, however, could deteriorate the surface morphology of the fibers. The other disadvantage of this type of electrospinning is the moderate choice of solutions in terms of the practical concentration of the polymer (usually in the range of 1-20%), since higher concentrations of the polymer could cause the high viscosity of the solution which reduce the spinability of the solution significantly. As mentioned before, the alternative for solution-based electrospinning is the application of the molten polymer. Although the main advantage of this method is the usage of solvent free approach which subsequently could result in the fabrication of bead free fibers with smooth surface morphology, the average diameter of the fibers is usually above 1μm with a very broad size distribution except in case of a few low-melting polymers [17]. Both approaches have been used and investigated vastly. For instance, Dalton et al. performed the melt spinning of Poly (ethylene oxide)-b-Poly (caprolactone)(PEO-b-PCL) on the living cells without any harm to cells. In general, high separation distance between the electrodes is used due to the high viscosity of the molten liquid. Therefore, a high electric field was required which increases the danger of the electric shock under normal atmospheric conditions [18]. Changing the atmospheric conditions in which the electrospinning is performed could alter the properties of the fibers significantly. It is expected that utilizing a high vacuum could produce fibers with enhanced properties since

4

higher electric field could be used. Rangkupan and Reneker achieved significantly thinner fibers with the melt spinning of Polypropylene (PP) under vacuum condition [19].

In comparison to the so called melt spinning, solution spinning has attracted more attentions due to its simplicity since no high temperature or high electric field are required as opposed to melt spinning. Various types of solution electrospinning have been developed mostly based on the configuration of the nozzle. Instead of utilizing a single nozzle, Ding et al. designed an electrospinning setup in which several syringes were used in parallel to feed a multi-nozzle electrode which was able to produce fibrous mats containing different polymers [20]. In an another study, Tomaszewski and his colleagues utilized a multi-nozzle system with various geometries as illustrated in Fig. 1-3.
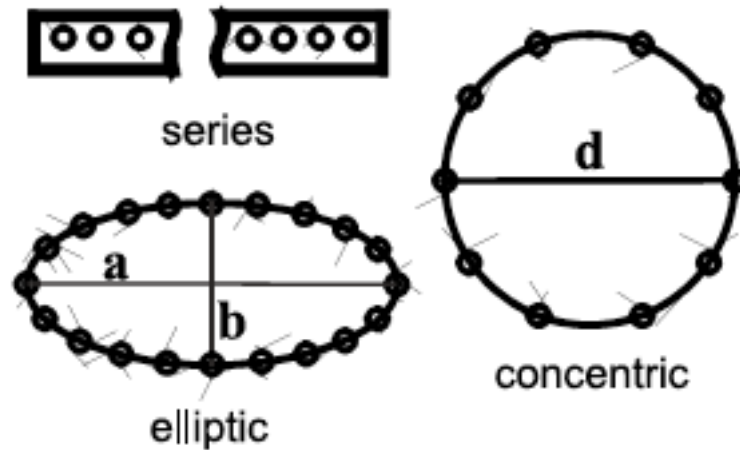
Fig. 1-3. The schematic of the muti-nozzle electrodes with different arrangements of series, elliptic and concentric [21].

Tomaszewski and his co-workers investigated the efficiency of the above-mentioned multi-nozzle systems by means of standard weighing procedure. Moreover, they examined the thickness and the morphology of the fabricated mats

by means of scanning electron microscopy. Their results indicated that the concentric configuration has the highest efficiency since it was able to produce 1 mg of Poly (vinyl alcohol) (PVA) in one minute with an acceptable morphology [21]. One of the most important advancements in the nozzle configuration used for solution electrospinning was the introduction of coaxial nozzles which are able to produce the so called core/shell fibers. Fig. 1-4a and Fig. 1-4b illustrates the configuration of a coaxial nozzle and the resultant Taylor cone, respectively. More details and also the application of the coaxial electrospinning will be discussed in chapter 2.
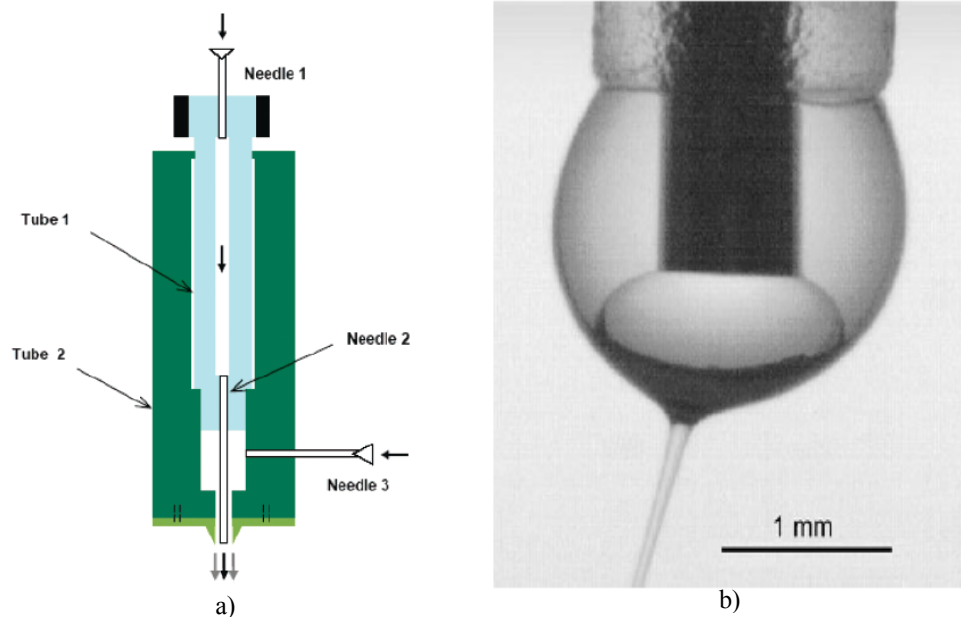
Fig. 1-4. a) The schematic configuration of a coaxial nozzle [22] b) The formation of the two Taylor cones at a coaxial nozzle. The image clearly illustrates the encapsulation of an internal Taylor cone in the external Taylor cone [11].

1.4. Application of electrospinning

As mentioned in section 1.1, the very first industrial application proposed for non-woven electrospun mats was filtration in textile industry. Since then, numerous applications have been investigated for electrospinning such as biomedical, sensing, composite reinforced fibers, etc. In the following sections we will discuss the most studied applications of the electrospinning.

1.4.1. Filtration and water purification

The application of electrospun fibers as efficient filters has been well-established long time ago. Due to the small size of the fibers, London-Van Der Waals forces play a significant role to enhance the capture of particulates in the medium [23]. One of the superiority of the fibrous mats in filtration over mats from conventional techniques is the higher porosity and the interconnected pore structure of the fibers which enhance permeability of the medium through the filter [24]. It is believed that the removal of the particulate matters by means of electrospun fibers could occur through one of these mechanisms: inertial interception, Brownian diffusion and flow-line interception [25,26]; however, the detailed information on these mechanisms could be the subject of other reports. Bjorge et al. applied the concept of electrospun fibrous mats utilizing various polymeric solutions in order to treat the water as a medium with focus on three different applications namely the removal of pathogens, the treatment of the wastewater in a laboratory-scale submerged membrane bioreactor (MBR) and finally, the clean water permeability (CWP) and the strength of the membranes.

The results regarding the pathogen removal efficiency of the fibers indicated that although the removal efficiency of the non-functionalized membranes was unsatisfactory, functionalizing the membranes with silver nanoparticles and also biocide could increase the efficiency significantly. The results of submerged MBR suggested that as a result of irreversible biofouling which occurred on the membrane, the flux decayed significantly as a function of time. Therefore, these membranes could not compete with the available commercial products [27]. In a similar study, Dotti and his co-workers investigated the feasibility of the electrospinning of various polymers such as PVA on ordinary filters of non-woven Poly (ethylene terephthalate)(PET) microfibers and their applications in air filtration. The flow resistance of the fabricated membranes were investigated using the air permeability measurements. The results showed that all membranes are comprised of fibers in the range of 70-500 nm. The air permeability measurements indicated a decrease due to flow resistance that could be controlled by means of the thickness of the membrane and the pore size of the fibers [28].

Photodegredation and removal of various contaminants by means of photocatalysts, especially titanium-based photocatalysts, from water have been extensively investigated in the last decades [29]. In spite of significant advancements in this area, the industrial application of these photocatalysts is still not feasible due to many technological obstacles. The most important obstacles are related to the removal of the catalysts powders and the recovery of them from the medium, the low activity of the catalysts and the inefficient distribution of the catalysts powders through the medium [29-31]. A new era of investigations began

8

with the introduction of composite nanofibers, specially the incorporation of the semiconductor nanoparticles into electrospun fibers. Laera et al. investigated the adsorption and photocatalyst activity of the commercial Degussa P25 photocatalyst incorporated into nanofibers against anionic azodye Congo Red and recalcitrant pharmaceutical Carbamazepine in saline water and in real municipal effluent. The result indicated that the P25 photocatalyst embedded in the fibers decreased the concentration of the both contaminants in the both media significantly [32].

1.4.2. Gas sensors

Generally, gas sensors could be defined as sensors that detect target molecules in the environment, especially when they are harmful for humans. Since the main features of the conventional chemical gas sensors such as selectivity, sensitivity, durability, reproducibility, response time, etc. are significantly influenced by the type of the absorbed molecules on the surface, considerable attention has recently been attracted towards the development of novel gas sensors [33-35]. Various types of materials such as polymers [36,37], semiconductors [38,39], composites [40,41], etc. have been used in order to sense the target gas molecules based on their chemical interactions. It is worth mentioning that the sensitivity of gas sensors could be improved significantly by increasing the surface area of the materials utilized for sensing [42,43]. Therefore, many attempts have been made to fabricate sensors with nanostructured sensing materials. Amongst all techniques to fabricate nanostructures for gas sensing, electrospinning has gained lots of attentions due to its capability of fabricating

various kinds of nanofibers with small diameter and high surface area and ability to produce different composites material. Generally, gas sensors could be designed based on variations in mechanical (acoustic), electric, photoelectric and optical properties of the transducer. However the details of principles of sensors is out of the scope of this report. Electrospun fibers with polyelectrolyte components, semiconductors and conducting polymers have been successfully designed and utilized for gas sensing with different configurations of fibers such as single fibers, hollow fibers, aligned fibers, nonwoven mats, etc. [44].

One of the most important devices using the properties of acoustic waves is Quartz Crystal Microbalances (QCMs). The QCMs have been utilized extensively to detect nanograms of various gases with high sensitivity and robustness [45]. Ding et al. utilized the electrospinning to deposit different composites containing different weight percentages of poly (acrylic acid) (PAA) and PVA with the average diameter of 100-400nm on QCM and characterize the sensitivity of the system against NH_3. Fig. 1-5 illustrates the schematic of a flow-type system normally utilized for polyelectrolyte nanofibers gas sensors.
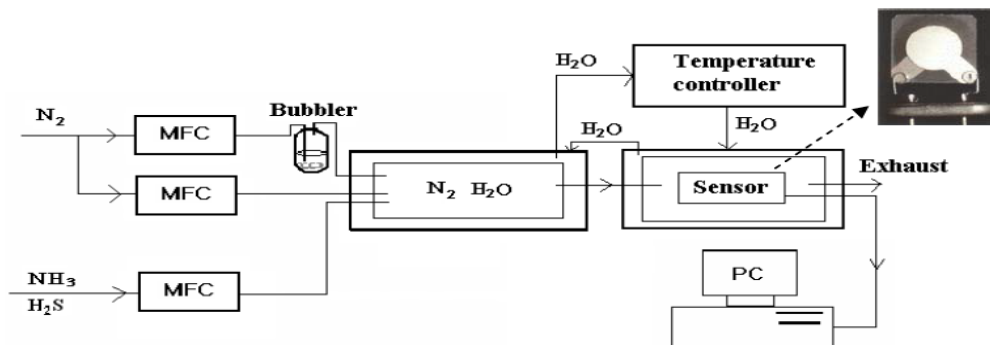
Fig. 1-5. The schematic of a flow-type system which could be used for gas sensing with polyelectrolyte nanofibers [46].

Despite the fact that PAA interacts with NH_3 strongly, the fabrication of nanofibers by means of the electrospinning from pure PAA is difficult due to the formation of strong hydrogen bonds between water molecules and large amount of carboxyl groups in PAA. Therefore PVA was introduced as a template and subsequent heat treatment was utilized to induce the crosslinking between PAA and PVA and reinforce the insolubility of the fibers. Afterwards, the nanofibers coated QCMs were utilized in a flow-type system illustrated in Fig. 1-5 for sensing measurements against dry N_2, wet N_2 and ammonia. The sensing of the gases was determined from the resonance frequency shifts of QCM. The results showed a large frequency shifts for NH_3 when PAA was present. However, the amount of PAA, the concentration of NH_3 and the relative humidity in the testing gas should be controlled carefully to avoid interference [47]. In order to utilize the principles of electrical resistance variation for gas sensing, Wei et al. successfully used ZnO normal nanofibers and also hollow fibers. A side heated gas sensor was designed by inserting Ni-Cr heating wire into a tube and depositing the fibers around the tube. Sensitivity, selectivity and durability of the designed sensor were investigated using the change in the resistivity as the function of acetone concentration. It is worth mentioning that in all the results described below, ZnO-1 refers to normal ZnO fibers, and ZnO-2 refers to ZnO hollow fibers. As illustrated in Fig. 1-6a the response of the both systems reached a maximum at 220°C which is the temperature at which adsorption of the acetone molecules on the surface of the fibers was more than with the desorption from the surface. Fig.

1-6b compares the response of the each system against various concentrations of the acetone.

Higher sensitivity of the sensor was observed for ZnO-2 sensor even for the concentrations of acetone as low as 1ppm, as illustrated in Fig. 1-6b Higher sensitivity of the ZnO-2 sensor was contributed to the higher specific area due to the formation of the hollow fibers. Fig. 1-6c illustrates the selectivity of the designed sensor for acetone at 220°C since the adsorption and desorption is temperature dependent and it is different for different gases. Finally, from Fig. 1-6d, it is clear that the durability of the ZnO-2 sensor is high since the signal remained constant for a period of 60 days [47].
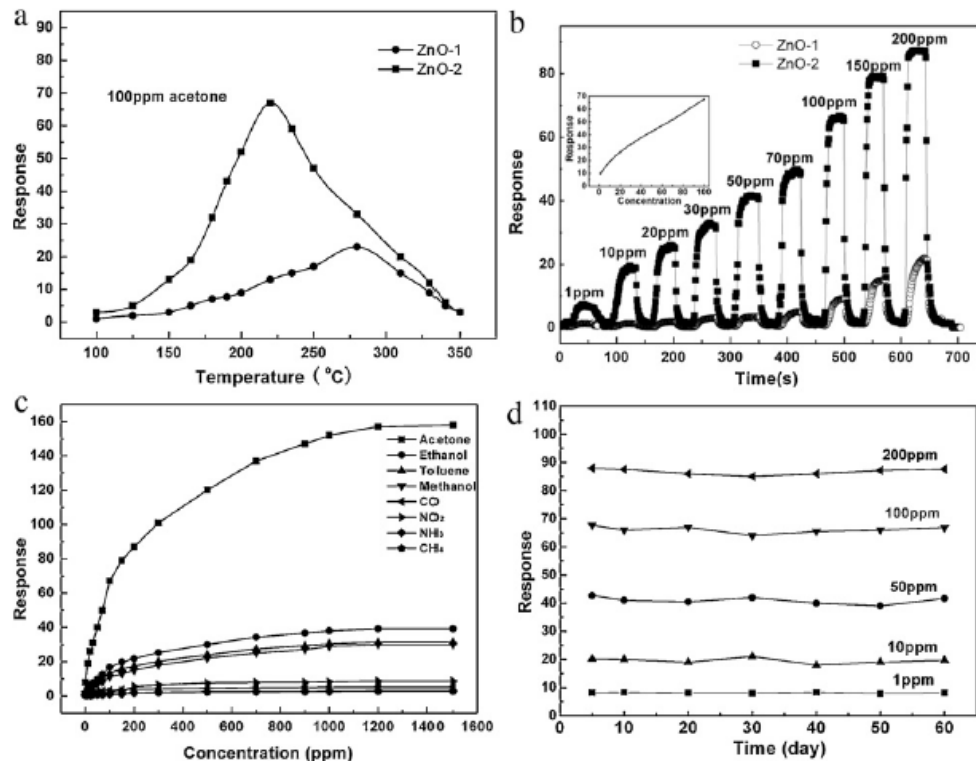
Fig. 1-6.a) Dependence of the response of the ZnO-1 and ZnO-2 sensors to temperature b) the change in the response and the recovery of the ZnO-1 and ZnO-2 sensors for different concentrations of the acetone c) the selectivity of ZnO-2 sensor d) the durability of the ZnO-2 sensor [47].

1.4.3. Biomedical applications

Amongst all applications of electrospinning, biomedical applications of the electrospun fibers are the most investigated applications. The increasing number of the papers and review articles investigating biomedical application of the electrospinning is an undisputed evidence of this fact. Vasita et al. has reviewed the current techniques for the fabrication of electrospun fibers and their application in different areas of biomedical engineering, especially for tissue engineering and drug delivery applications [48]. In a similar review, Laurencin et al. have reviewed the patents on the use of electrospun fibers for biomedical applications [49]. Below, application of the electrospinning in the two most important areas of biomedical engineering are described ,i.e. tissue engineering and drug delivery.

1.4.3.1. Application of electrospun fibers in tissue engineering

Tissue engineering or regenerative medicine is an interdisciplinary science involving various fields of study such as medicine, biology, materials science and engineering. Basically, the main goal of tissue engineering is to provide scaffolds which are capable of accepting and regenerating cells for tissues compromised by diseases, injuries, etc. The main feature of these scaffolds is that they should not stimulate any immune responses [50]. The reason why electrospun fibers have been attracting lots of attentions is the loose 3D porous structure of the fibrous mats that can mimic the extra cellular matrix (ECM) perfectly. The role of the natural ECM in the body is to separate different tissues, provide anchorage to the

cells and form a supportive network around cells. That is why electrospun fibrous mats are perfect candidates for this application. It is worth noting that the fibers utilized for tissue engineering should be biocompatible and biodegradable since no immune system stimulation should occur. Moreover, the ECM fabricated from electrospun fibers should degrade with time and be replaced by new naturally
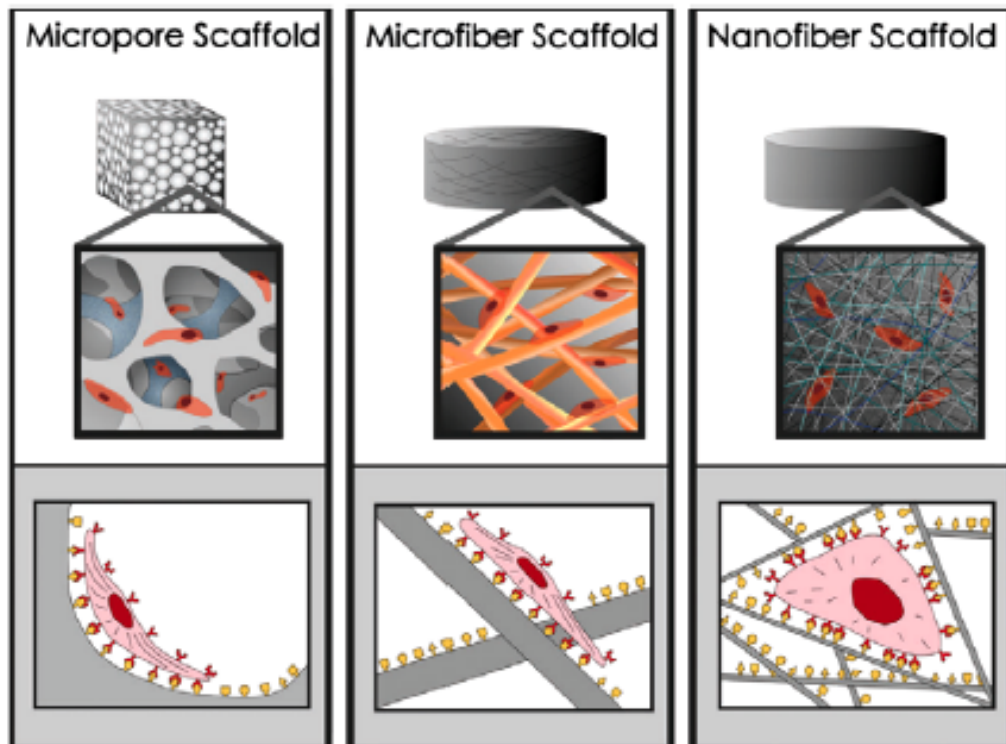
Fig. 1-7. Different fibrous architecture could be used for tissue engineering [51].

regenerated tissue [50]. The other important factor which should be controlled is the architecture of electrospun mats as illustrated in Fig. 1-7. The scaffold structure could significantly influence the cell bindings to the scaffold. Microscale structure of scaffold flattens the cell since it has lower number of binding site. On the other hand, nanostructured scaffolds have higher surface area that can provide much more binding sites to cells [51]. Numerous studies have been carried out to

investigate the efficiency of the various types of fibrous mats to be utilized as scaffolds for different types of cells. Table 1-1 summarizes the type of polymers and the type of the cells used in different studies.

Table 1-1. Various types of polymeric solutions utilized as scaffolds for different kinds of cells.

Polymeric solutions	Cells	Reference
Poly (urethane) (PU)	Smooth muscles cells	[52]
Poly (phosphazenes)	Endothelial cell	[53]
Poly (propylene carbonate)	Bone marrow mesenchymal stem cells	[54]
Poly (ester urethane)	Fibroblasts	[55]
Poly (lactide-co-glycolide)(PLGA)/amorphous tricalcium phosphate	Human mesenchymal stem cells	[56]
Poly (L-lactide)-hydroxyapatite (PLLA/HA)	Osteoblast cell MG-63	[57]

Extensive studies have been carried out to investigate the efficiency of electrospun fibers for tissue engineering. For instance, Li et al. successfully fabricated silk fibroin fiber scaffolds containing bone morphogenetic protein 2 (BMP-2) with and without hydroxyapatite nanoparticles (nHAP) through the electrospinning process. Afterwards, the fabricated scaffolds were utilized for in vitro bone formation from human bone marrow-derived mesenchymal stem cells. Three different scaffolds were prepared with the combination of silk, PEO, BMP-2 and nHAP. First and second samples were fabricated by using only BMP-2 in silk/PEO and only nHAP in silk/PEO. The last sample was prepared by adding both BMP-2 and nHAP to silk/PEO. Positive control samples were fabricated by

electrospinning the blend of silk/PEO and silk/PEO-extracted solutions in order to investigate the effectiveness of BMP-2 and nHAP in the formation of mesenchymal stem cells. The results indicated that the scaffolds containing BMP-2 showed higher degree of calcium deposition as well as improving the transcription level of bone-specific markers compared to the control samples. Moreover, the samples containing both BMP-2 and nHAP showed higher degree of calcium deposition and transcription level of the markers [58]. The role of nHAP in cell binding and attachment to the scaffolds was established previously. Cells normally bind to ECM proteins such as vitronectin by means of the intergins. Improved adsorption and adhesion of the intergins to the surface of the hydroxyapatite was attributed to be the main reason for higher adhesion of the cells to nHAP [59].

1.4.3.2. Electrospun fibers as drug delivery systems

Generally, the area of drug delivery could be defined as a related area of study to tissue engineering in which the release of the drug could assist the regeneration of the tissue. Goldberg et al. have reviewed various structures, especially nanostructured materials that could be used in drug delivery as well as tissue engineering [60]. One of the most important areas of the study when drug delivery systems are considered is the controlled drug release therapy. Controlled release drug therapy is a process in which a predetermined concentration of a drug is delivered to a particular target over a specified duration, in a predicted behavior [61]. The main goal of this process is to increase the effectiveness of the drug by means of localizing the delivery, decreasing the side effects, decreasing the

number of the administrations and even removal of the need for specialized administration methods [61,62]. Numerous studies have been carried out in order to design, characterize, and develop controlled drug delivery systems. The focus has been aimed in particular towards drug delivery systems that utilize biodegradable polymers such as different grades of poly (lactic acid)(PLA) [63-66]. Fortunately, the advances in nanotechnology have offered various structures for incorporating different therapeutic agents into these biodegradable polymers including nanocapsules, nanoparticles, micellar systems, etc. [67,68]. In a recent study, Koutsopoulos et al. investigated the controlled release of various functional proteins from a peptide hydrogel scaffold. They were able to successfully incorporate different proteins such as bovine serum albumin (BSA), lysozyme, etc. into a designed hydrogel scaffold and study the release kinetics of the drugs using the fluorescence correlation spectroscopy (FCS) technique. It was concluded that their biodegradable and injectable designer self-assembling peptide hydrogel scaffold could satisfy the controlled release drug therapy concept ,i.e. sustained drug release [69].

Introduction of the electrospinning technique to the controlled release drug therapy inspired a new era of investigations in which the incorporation of the drug into electrospun fibers could result in the fabrication of effective drug delivery systems. The details about the drug delivery systems based on the electrospun fibers and different types of these systems are discussed in chapter 2.

1.5. Listeria and Listeriosis

Listeria is a bacterial genus, gram-positive bacilli, containing seven species of *L. grayi, L. innocua, L. ivanovii, L. monocytogenes, L. murrayi, L. seeligeri,* and *L. welshimeri.* It has been named after the pioneer of the sterile surgery, Joseph Lister. However, the genus gained its current name at 1940. Table 1-2 summarizes the scientific classifications of Listeria.

Table 1-2. The scientific classifications of Listeria.

Scientific classifications	
Kingdom	Bacteria
Division	Firmicutes
Class	Bacilli
Order	Bacillales
Family	Listeriaceae
Genus	Listeria

Fig. 1-8 illustrates the scanning electron micrograph of a Listeria *monocytogenes.* Under the microscope, all of the species of Listeria appear as small, gram-positive rods which sometimes are arranged in chains.

Fig. 1-8. The micrograph of Listeria *monocytogenes*[70].

Among all the species of Listeria, *L.monocytogenes* is the only pathogenic species which could cause Listeriosis that is a fatal food borne infection [70]. It has been reported that the rate of incidence of Listeriosis is much lower compared to other food borne diseases results from *Escherichia coli* (*E.coli*) and *Staphylococcus*. However, Listeriosis has the highest fatality rate (up to 40%)[71]. Listeria could be found in soil which could cause contamination in vegetables and fruits such as cantaloupe [72]. Moreover, animals could carry Listeria and, therefore it could be found in uncooked meat, pasteurized and unpasteurized milk, milk products, and processed foods.

Chapter 2: Literature review

In the previous chapter, an overview on the basic concepts of the electrospinning and its various applications was delivered. The purpose of this chapter is to discuss the process of electrospinning in greater details. Moreover, the application of the electrospun fibers in designing drug delivery systems will be debated extensively.

2.1. The electrospinning process

As stated previously, the process of electrospinning involves the application of a sufficiently high voltage to a polymeric droplet which is suspended from a metallic nozzle. The pioneering observations by G. I. Taylor and his colleagues indicated that applying high voltage to a polymeric droplet could change the spherical shape of the droplet to a conical shape, named the Taylor cone after G. I. Taylor [73] (Fig. 1-2). The main reason for this change in the shape is believed to be the competition between the surface tension of the droplet and the electrostatic forces caused by the external electric field [74]. If the applied voltage is sufficiently high that the surface tension of the droplet is overcome by the electrostatic forces, a polymeric stream (called the jet) is ejected from the cone and travels towards the collector. The observations of Baumgarten and Warner et al. lead to the conclusion that the jet goes through a series of bending processes contained in a conical envelope. These bending processes follow complex routes, called bending instabilities [75,76]. Undoubtedly, some of the main contributions to the basic understanding of the electrospinning process

were made by the works of Darrel. H. Reneker. Utilizing an electrospinning system equipped with a high-speed camera, Reneker and his colleagues were able to investigate the behavior and the role of the bending instabilities in an electrospinning process [77]. Fig. 2-1 illustrates the schematic of the system used by Reneker.
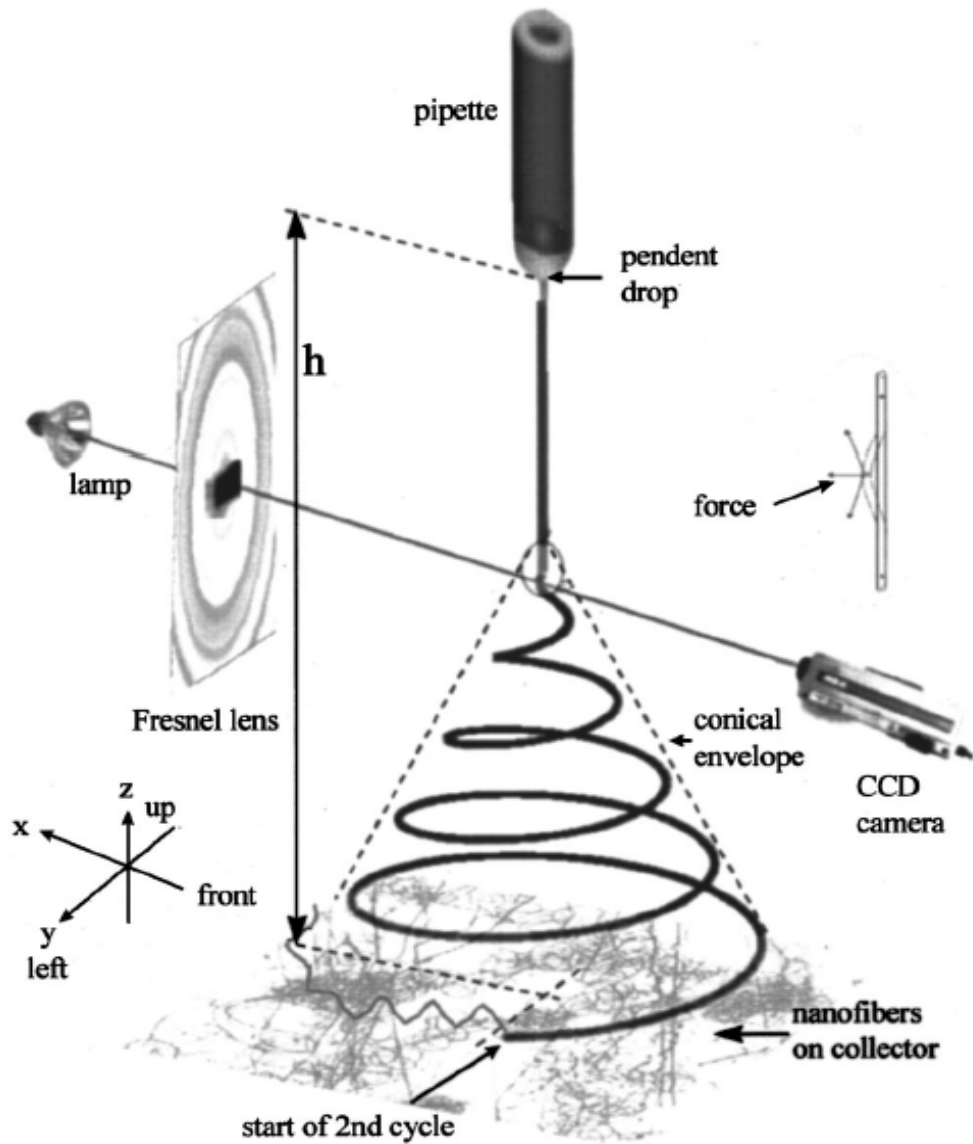
Fig. 2-1. The schematic of the electrospinning system equipped with the high-speed camera to observe the bending instability process [77].

The observations made by Reneker et al. on the formation of the Taylor cone confirmed Taylor's statement that the instability of the droplet occurs when the applied voltage is high enough for the electrostatic forces to exceed the surface tension of the droplet. Above this voltage threshold, a continuous jet was ejected from the Taylor cone which carries the excess charges, flies toward the collector and finally is deposited on the ground collector.

The jet path was investigated by adjusting the camera to focus on the vertex of the conical envelope. The camera was able to produce images with a speed of 2000 frames per second. Fig. 2-2 illustrates the conical envelope during the electrospinning process and demonstrates the evolution of the jet.

10 mm
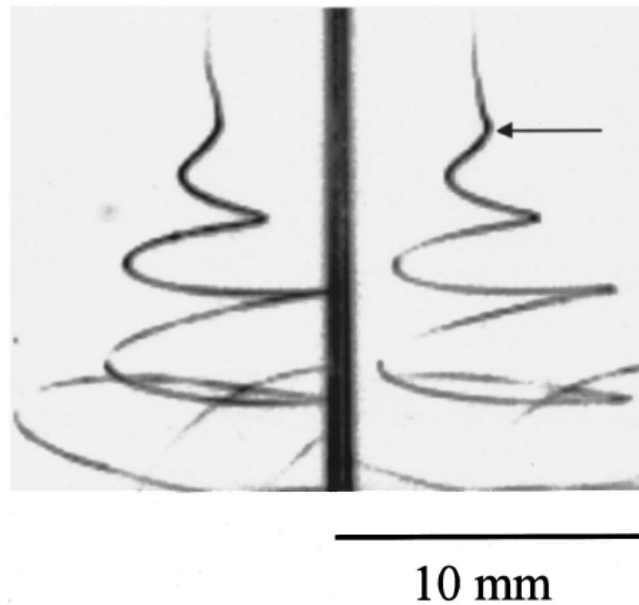
Fig. 2-2. The evolution of the jet in the electrospinning process. The formation of the conical cone is the direct consequence of the bending instabilities [77].

The spiral path illustrated in Fig. 2-2 is a typical path that the jet undergoes during the electrospinning process. After a short straight segment, the

jet enters a bending, spiraling, winding and looping route in which the jet stretches in length and narrows in diameter as the circumference of the loop increases. The end point of the initial straight segment is marked by an arrow in Fig. 2-2. Furthermore, during the evolution of the jet in the shape of the conical envelope, segments of the loop leave the route of the primary loop and develop a new instability, in a direction different from the initial path and on a smaller scale. This is illustrated in Fig. 2-3.
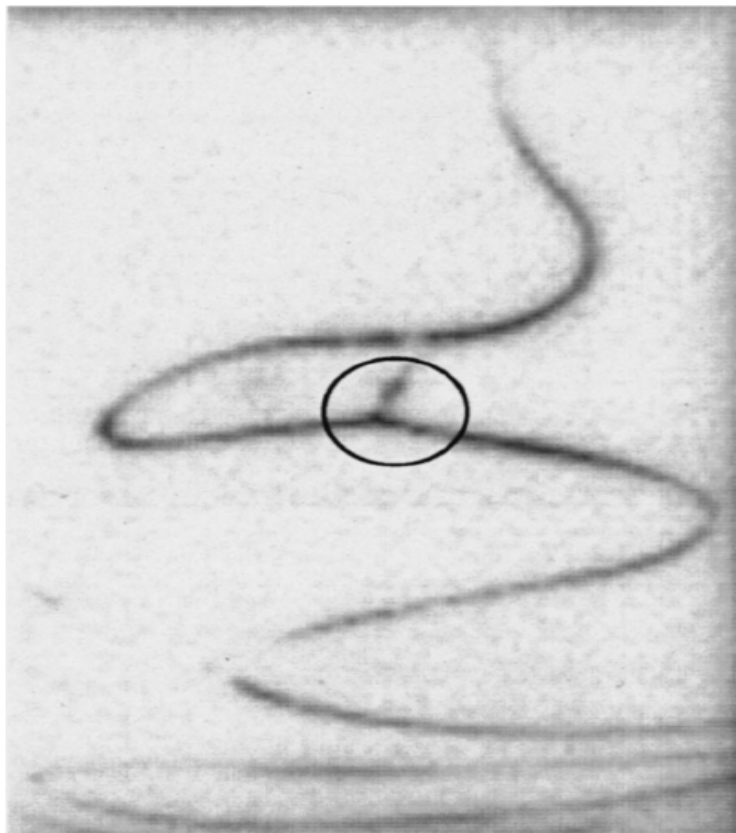
5 mm

Fig. 2-3. The development of the new bending instability from the initial conical envelope in smaller scale [77].

Based on the observations of Reneker et al., a bending instability cycle can be described in three stages:

I. A straight or slightly curved segment forms at the vicinity of the Taylor cone which subsequently splits into an array of bends as illustrated in Fig. 2-4;
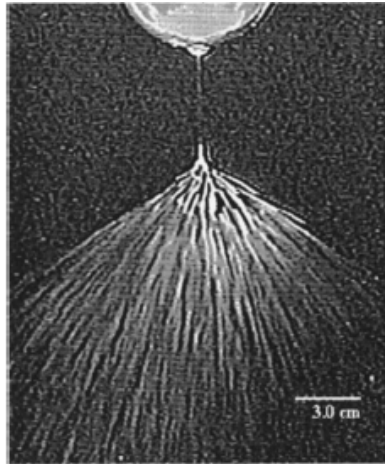
Fig. 2-4. The split of the straight segment into an array of bends [77].

II. The jet in each bend stretches and the array of bends evolves into a series of spiraling loop with growing diameter;

III. As the circumference of the loop increases, the diameter of the jet in the loop decreases. At specific points, the conditions for the occurrence of step I are established and the cycle repeats itself by splitting the jet into a smaller array of bends. In other words, the cycle occurs in smaller scale.

Reneker concluded that the jet diameter could decrease further, even to a nanometer scale, if more cycles occur [77]. It is worth noting that based on these observations, the most important parameters that could affect the diameter of the jet are the fiber thinning due to the electrostatic forces and also the number of

bending instability cycles that the jet undergoes. More details on the effect of these parameters are presented with experimental data in Section 4.1.

2.2. Effective parameters in the electrospinning process

Electrospinning is a process encompassing various electrostatic and hydrodynamic phenomena. Therefore, numerous parameters are involved which could affect the electrospinning process. Commonly, the effect of these parameters is discussed in terms of the influence on the diameter, the size distribution, and also the morphology of the fibers. Generally, these parameters could be categorized into two groups: parameters related to the materials such as polymer (type and molecular weight), solvent (type, vapor pressure), solution properties (the concentration of the polymer, rheological behavior, viscosity, surface tension); and, processing parameters such as the applied voltage, the distance between the nozzle and the collector, the diameter of the nozzle, the pumping rate of the solution and the ambient conditions (temperature, humidity). Several investigations have been carried out to determine the effect of these parameters on an electrospinning process and numerous models have been proposed. Table 2-1 summarizes few references which introduced models for the electrospinning and electrified jet with their features. In an extensive study, Thompson et al. investigated the effect of 13 materials and processing parameters on the size of the fibers and determined the sensitivity of the change in diameter to each parameter.

Table 2-1. Models proposed in the references for the electrospinning process and their feature.

Reference	Features
[78,79]	Linear stability analysis of small capillary and bending of electrified viscous Newtonian jet
[80-82]	Linear and non-linear model of the dynamics of single and multiple bending jets in an electrospinning process. The model discusses the solution viscoelasticity, electrostatic forces, surface tension, jet-jet interactions and solvent evaporation and solidification.
[83]	Straight electrified jet of viscoelastic liquid

The results regarding the study of Thompson et al. on the effect of various parameters indicated that all the parameters could be categorized into three groups based on the sensitivity of the diameter of the fibers to each parameter. The distance between two electrodes, initial jet radius, volumetric charge density, viscosity and relaxation have the greatest effect, while solution density, polymer concentration, applied voltage, perturbation frequency and solvent vapor pressure have moderate impacts. Other factors such as humidity, surface tension and vapor diffusivity are of less significance [84]. The effect of various parameters including the applied voltage, polymer concentration, feeding rate, etc. on the diameter and the length of poly (caprolactone) (PCL) nanofibers were studied by Beachley [85]. It was concluded that the feeding rate of the polymeric solution did not have a significant effect on the diameter and the length of the fabricated fibers; however, utilizing excessively high feeding rate should be avoided since it could cause the accumulation of excess polymer at the tip of the nozzle and halt the

26

electrospinning process by solidification at the tip. Moreover, the effect of the polymer concentration in the solution was investigated by fixing all the parameters and changing the concentration of the polymer between 8% and 20%. It was concluded that the maximum length and diameter of the fibers could be achieved by utilizing higher concentrations of the polymer and the degree of the change in the length and diameter is significant; however, increasing the concentration increases the viscosity of the solution which subsequently could cease the process. Furthermore, the effect of the voltage on the length, diameter and the uniformity of the fibers was studied by increasing the voltage from 10kV to 20kV. The results indicated that although both the length and diameter of the fibers decreased by increasing the voltage, the effect of the applied voltage was more significant on the diameter. In addition, the uniformity of the fibers increases when the voltage was increased from 10kV to 20kV.

Considering Eq. 2-1 stated below, one could conclude that controlling the applied voltage (v) and also the distance between the nozzle and the target (d) is crucial since these two parameters could be combined to generate the electric field (E) which in turn controls the electrostatic forces applied to the jet.

$$E = \frac{v}{d} \qquad (2-1)$$

Numerous studies have been carried out to understand the effect of the applied voltage and the distance between the nozzle and the collector on the electrospun fibers. These effects have been studied in terms of the size of the fibers and also the size distribution. For instance, Tan et al. investigated the effect

of various parameters including the applied voltage on the formation of the fibers. The results indicated that although parameters such as the concentration of the polymeric solution affected the diameter of the fibers significantly, no noticeable change was observed in the diameter when changing the applied voltage from 10kV to 20kV [86]. Similar results were obtained from previous investigations in which the effect of applied voltage on the diameter was found to be insignificant [87-90]. Megelski et al. investigated the effect of the separation distance between the nozzle and the collector on the diameter and the morphology of the poly (styrene) (PS) fibers by changing the distance from 10cm-35cm with 5cm increments. The results implied that although the distance did not show a significant effect on the diameter of the PS fibers, the morphology of the fibers underwent a considerable change. Decreasing the distance only by 5cm from 35cm initiated the formation of scattered elongated beads along the PS fibers [91].

However, as reported by Heikkilä et al. the optimum conditions of the applied voltage and distance for obtaining the finest fibers as well as the narrowest size distribution of the fibers are often contradictory in different studies [92]. A decrease in the average diameter of fibers was observed with an increase in the applied voltage [93,94]. Also, an increase in the average diameter was reported with the increase in the applied voltage in other studies [95-97].

2.3. Drug delivery systems based on the electrospun fibers

2.3.1. Types of drug delivery systems

As discussed in Section 1.4.3.2, the introduction of electrospun fibers to the area of controlled release drug therapy initiated a new era of investigations. Generally, two types of drug delivery systems could be designed by means of the electrospun fibers: matrices type and reservoirs type [98-100]. Fig. 2-5 illustrates the schematic of the configuration of each type. As depicted in Fig. 2-5A, the therapeutic agent is dispersed homogenously in the electrospun fiber matrix when the matrices type drug delivery system is considered.
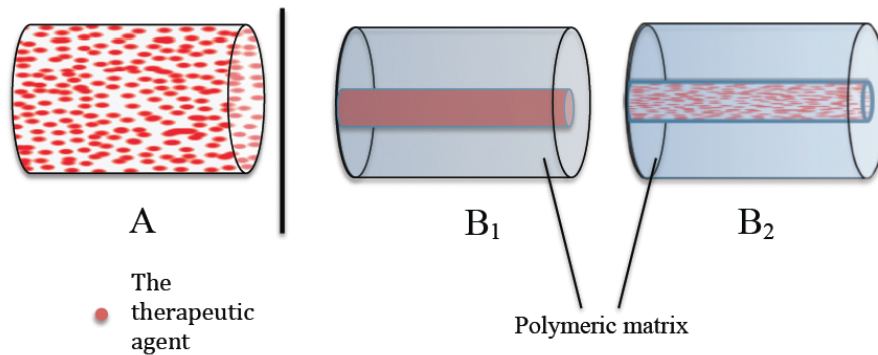
Fig. 2-5. Possible configurations for designing the drug delivery systems by means of electrospun fibers (A) The drug is dispersed through out the fiber matrix homogenously (B$_1$) Core/shell fibers with the pure drug as the core (B$_2$) The therapeutic agent is dispersed in the fiber matrix as the core is shielded by another polymer.

Drug release investigations on this type of systems indicate that the release of the therapeutic agent undergoes an initial burst release followed by a constant decrease in the release rate due to the fact that the agent requires a longer diffusion path to release. In a study by Ji et al., the release pattern of BSA

incorporated into PCL prepared by blend electrospinning was investigated. The results indicated an initial burst release for the fibers. The drug release continued by a progressive decrease in the release rate until the system reached its maximum drug release [101]. In a similar study, Kenawy and his colleagues designed a drug delivery system based on the incorporation of ketoprofen into PCL as a biodegradable polymer, PU as a non-biodegradable polymer and a blend of both by means of blend electrospinning. The aim of their study was to investigate the drug release and the mechanical properties of each system. Their results depicted that although the mechanical properties of the system that utilized the blend of PCL and PU has superiority, the drug release of all systems followed the same path of initial burst release [102].
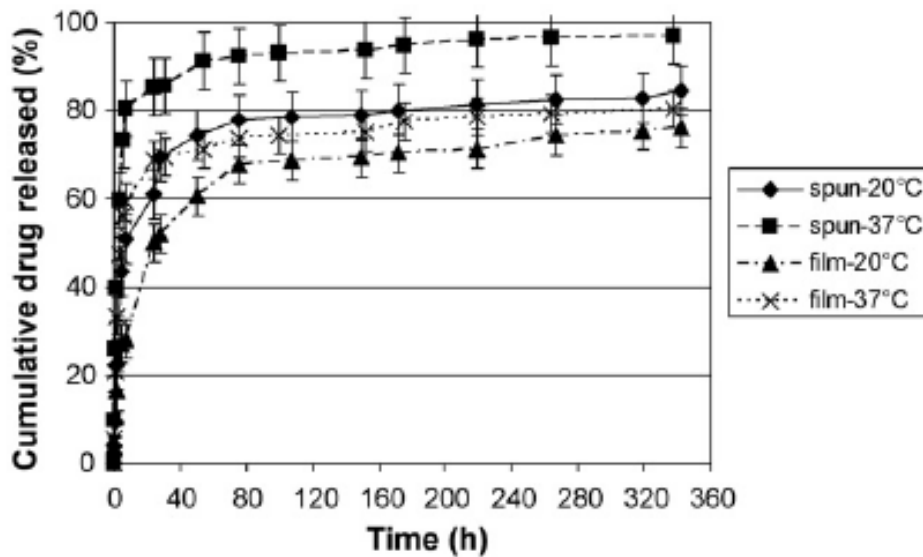
Fig. 2-6. In vitro drug release from fibers and polymeric films incorporated with ketoprofen in the buffer solution at 20°C and 37°C [102].

As illustrated in Fig. 2-6, a higher concentration of the drug was released from the fibers at any given time and temperature compared to the drug released

from the films; however, in all the designed drug delivery systems, the burst release was observed which was responsible for the release of the most of the drug in the first few hours.

The major drawback of the aforementioned blend electrospinning for designing drug delivery systems is the initial burst release of the therapeutic agent that causes the efficiency and the lifetime of the system to deteriorate [103,104]. As opposed to the matrices type drug delivery systems, reservoir type systems utilize a core/shell structure in which the drug-incorporated polymer is shielded by another layer of the polymer, as illustrated in Fig. 2-5B. Many studies have been carried out in order to design and characterize reservoir type drug delivery systems. For instance, Moreno et al. successfully encapsulated lactate dehydrogenase as a model drug in PVA through a coaxial electrospinning process. They observed that the system is capable of releasing the drug in a sustained manner within a period of one month [105]. Liao et al. utilized the concept of coaxial electrospinning in order to encapsulate the model protein i.e. BSA, into the Poly (ethylene glycol)(PEG) core polymer. The aim of their study was to obtain BSA in the shape of the fibers. Since BSA is not spinnable, the use of core/shell structure could give the ability of spinning to BSA. Moreover, the encapsulation of proteins such as BSA in the core/shell structure could retain the bioactivity of the proteins. The drug release investigations indicated that the protein was released in a sustained manner over a period of 40 days for all the designed drug delivery systems. Furthermore, the bioactivity of the protein did not deteriorate during the process [106].

Coaxial electrospinning has been established as an effective method to encapsulate the therapeutic agent. As stated before, utilizing coaxial electrospinning in order to design drug delivery systems holds many advantages over the blend electrospinning such as the suppressed burst release, prolonged life time of the system and the protection of the therapeutic agent from harsh environments; however, the need for special equipment (coaxial spinneret), the limited choice of the polymeric solution and the need for a precise choice of the electrospinning parameters has not yet allowed this technique to be industrialized. The search for a new technique with the ability to produce drug delivery systems with the functionality of systems fabricated by coaxial electrospinning (i.e. controlled drug release) but with more a simple process led to the introduction of emulsion electrospinning. The most important advantage of this type of the electrospinning is that it utilizes only one nozzle as opposed to coaxial electrospinning. Furthermore, the technique is able to fabricate not only core/shell fibers, but also it is able to produce the beads-in-string structure. Fig. 2-7 illustrates the schematic of the electrospinning solution preparation for emulsion electrospinning technique. As depicted in Fig. 2-7, the first step in order to prepare a solution for emulsion electrospinning is to emulsify the core containing solution by means of vigorous stirring. Afterwards, the fiber forming material (polymer) is dissolved in the solution prepared in the previous step. The next step is to stir the mixture in order to get a homogenous solution. If simple electrospinning process is carried out utilizing the above-mentioned solution, core/shell fibers with the drug in the core could be obtained.
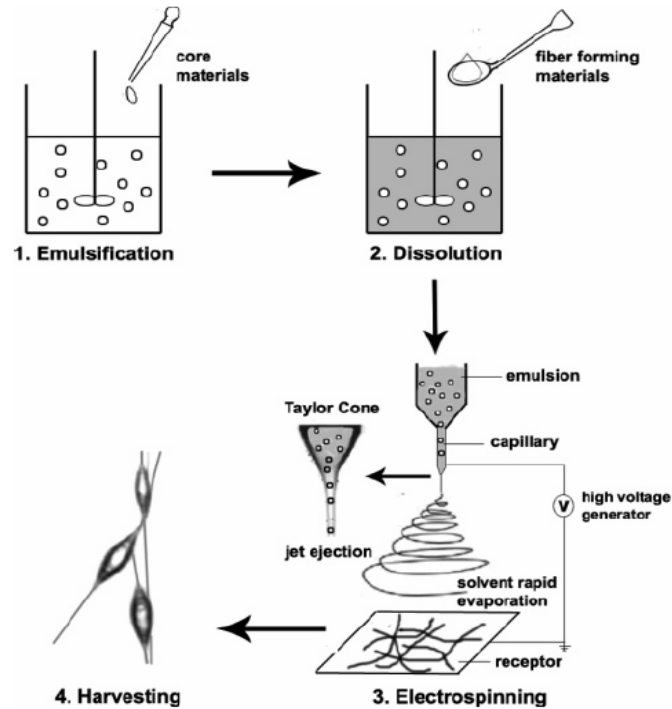
Fig. 2-7. Different steps in preparation of a solution for emulsion electrospinning [107].

Xu et al. investigated the formation of core/shell fibers utilizing the emulsion electrospinning approach. They were able to produce uniform core/shell fibers using the electrospinning of a water-in-oil emulsion in which the aqueous phase consisted of PEO in water and the oily phase comprised of the PEG-PLA diblock copolymer dissolved in chloroform. A mechanism was proposed to explain the formation of the core/shell fibers from the emulsion. Fig. 2-8 illustrates the schematic of the proposed mechanism. It was suggested that the stretching and evaporation induced de-emulsification is the main reason for the formation of the core/shell fibers [108].
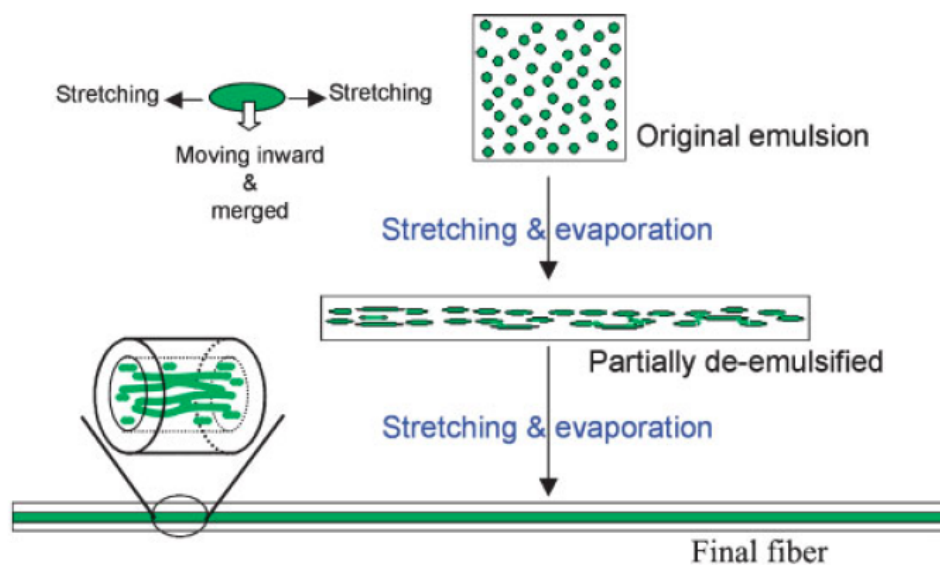
Fig. 2-8. The schematic of the formation of the core/shell fibers from the emulsion. The stretching and evaporation induced de-emulsification was proposed to explain the formation of the core/shell fibers [108].

Qi et al. utilized emulsion electrospinning to fabricate a beads-in-string structure. BSA was used as a model drug which was dispersed in Ca-alginate microspheres and subsequently incorporated into Poly (L-lactic acid)(PLLA) through an electrospinning process. SEM analysis confirmed the formation of the beads-in-string structure that proved the effectiveness of this technique for microencapsulation purposes. The protein release investigations on three different samples implied that the formation of the beads-in-string structure was the only structure with the ability of sustained drug release. Fig. 2-9 illustrates the release behavior of the BSA from different structures along with the morphology of each structure analyzed by SEM. It was concluded that using naked Ca-alginate microspheres resulted in the burst release of the BSA (approximately 80%) in the first few hours (Blue markers in the release graph).
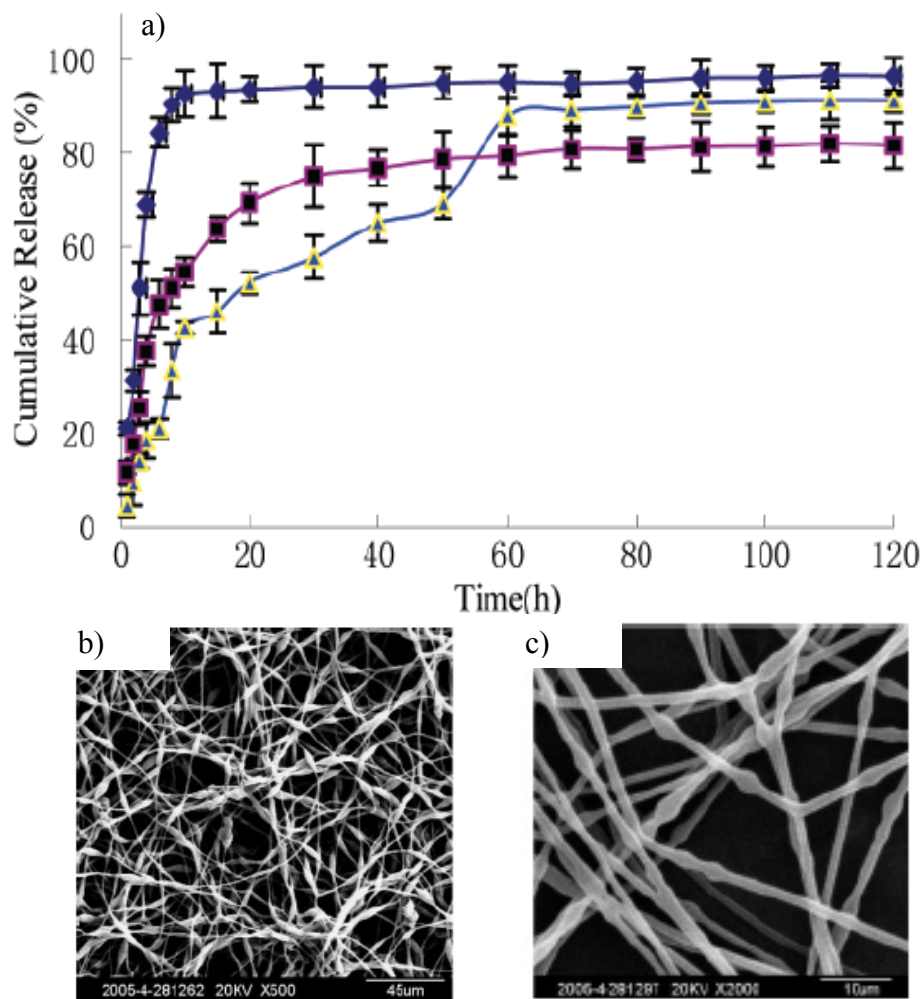
Fig. 2-9.a) The BSA release from the Ca-alginate microspheres (◆), fibers shown in b) (■) and beads-in-string structure illustrated in c) (▲) [107].

Applying the voltage of 20kV to the emulsion in the electrospinning resulted in the incomplete formation of the beads structure possibly due to the high evaporation rate of the solvent. This incomplete formation consequently caused the burst release of the BSA although the degree of burst release was lower than that of microspheres (violet markers). Applied voltage of 15kV appeared to be the optimized voltage since the formation of the beads-in-string structure occurred completely as illustrated in Fig. 2-9c. Moreover, the sustained

release of the BSA along with the suppressed burst release was observed for this system (yellow markers) [107].

2.3.2. Kinetics of the release

Numerous studies have been conducted to understand the release kinetics of a therapeutic agent from a matrix with various structures such as hydrogels, fibers, microcapsules, etc. Amongst all the proposed models, four mathematical equations could be utilized for almost all systems. Here in, these models are introduced briefly.

2.3.2.1. Korsmeyer-Peppas equation [109]

Korsmeyer and Peppas developed an empirical equation in order to predict the release kinetic and mechanisms from a polymeric matrix by means of the structural properties of the matrix. Generally, the release of the drug from a polymeric matrix through the dissolution of the polymer is limited to thin films. In addition, the drug release usually could be described by Fickian diffusion in which approximately 50% of the fraction of the release could be described by the square root of time. Korsmeyer and Peppas postulated Eq. 2-2 indicated below;

$$\frac{M_t}{M_\infty} = kt^n \qquad (2-2)$$

In which "$\frac{M_t}{M_\infty}$" is the fraction of the released drug, "t" is time and "k" is the release rate constant which is related to the structural and geometrical properties of the drug delivery system. "n" is known as the release exponent.

Korsmeyer and Peppas tabulated the value of "n" for different drug delivery structures and predicted the release mechanism as illustrated in Table 2-2.

Table 2-2. The predicted release mechanism based on the release exponent and the structure of the drug delivery system.

Release exponent (n)			Release mechanism
Cylindrical systems	Spherical systems	Thin film	
≤ 0.45	≤ 0.43	≤ 0.5	Fickian diffusion
$0.45 < n < 0.89$	$0.43 < n < 0.85$	$0.5 < n < 1$	Non-Fickian diffusion
≥ 0.89	≥ 0.85	1	Zero-order kinetics

2.3.2.2. Zero-order release kinetics

The zero-order release kinetics is a kinetics in which the concentration of the released drug in the medium is independent of the concentration of the drug embedded in the drug delivery system. Eq. 2-3 shows the equation applied to the zero-order release kinetics.

$$M_t = M_0 + kt \quad (2-3)$$

In the early investigations on controlled release drug therapy, the emphasis was put on designing the drug delivery systems with the ability to release the drug based on the zero-order release kinetics since it was believed that it could keep the concentration of the drug in the media (blood) constant; however, further analysis proved the inefficiency of this type of systems since the absorption of the drug in the body does not occur with the zero-order kinetics [110].

2.3.2.3. First-order release kinetics

The first-order release is referred to a release in which the released concentration of the drug is dependent on the provided concentration of the drug in the system at the designing stage. The main characteristic of the systems which follow the first-order release kinetics is that the concentration of the drug decreases exponentially as a function of time [111] as illustrated by Eq. 2-4.

$$Log(M_t) = Log(M_0) + \frac{kt}{2.303} \qquad (2-4)$$

It is believed that utilizing the drug delivery systems with first-order release kinetics could be beneficial in cases where higher degree of release is required compared to the zero-order kinetics due to the possibility of the rapid elimination of the therapeutic agent from the environment [112].

2.3.2.4. Hixon-Crowell release kinetics

Basically, Hixon-Crowell release refers to a drug delivery system in which the release of the drug occurs by means of the dissolution of the carrier. The basic principles of the dissolution was discussed by Noyes and Whitney in 1897 with a well-known equation stated below (Eq. 2-5):

$$\frac{dM}{dt} = \frac{DA}{h}(C_s - C) \qquad (2-5)$$

in which "$\frac{dM}{dt}$" describes the rate of the drug release, "D" is the diffusion coefficient of the therapeutic agent, "A" is the surface area of the system which is exposed to the media, "h" is the thickness of the system where diffusion occurs,

"C_s" is the solubility of the agent and "C" is the concentration of the agent at any given time in the media. The assumption utilized to derive Eq. 2-5 is that the surface area of the system remains constant during the period of the release; however, in many cases, the system dissolves in the media in order to release the drug. In other words, the surface area changes during the release process. Hixon and Crowell derived an equation which is normalized for the decrease in the surface area.

$$M_0^{\frac{1}{3}} - M_t^{\frac{1}{3}} = kt \quad (2-6)$$

It is worth mentioning that Eq. 2-6 is also known as the Hixon-Crowell cube root equation [113].

All above-mentioned models could be used to investigate the release kinetics for drug delivery systems; however, the model developed by Korsmeyer and Peppas has been used in many investigations since one could predict the mechanism of the release in addition to determining the kinetics.

2.4. Thesis objective

The thesis follows two main objectives. Firstly, an electrospinning setup is designed and assembled with the goal to replace the conventional Ac-Dc high voltage supplies with Dc-Dc modules to decrease the cost of the setup and also to increase the mobility. Also, the setup is optimized in terms of the applied voltage and the separation distance between the nozzle and the collector with the goal to obtain fine fibers with narrow size distribution. The second objective is to design

and characterize a reservoir type drug delivery system by means of the coaxial electrospinning and evaluate the effectiveness of the system in antibacterial applications.

- The detailed information on the design and assembly of the electrospinning setup is presented in section 3.2.1.
- The optimization of the system based on the effect of the electric field on the average diameter and the size distribution of the fibers by changing the voltage and distance is described in section 4.1.
- The characterization of the drug delivery system is presented in sections 4.2. to 4.6.
- The antibacterial application of the designed drug delivery system is discussed in section 4.7.
- Finally, a general conclusion along with the possible future directions is described in chapter 5.

Chapter 3: Materials and methods

The aim of this chapter is to introduce the materials utilized to conduct this study. Afterwards, the detailed experimental procedure is discussed.

3.1. Materials

In order to fabricate the core/shell nanofibers and also the normal nanofibers, Nylon6 and poly (methyl methacrylate) (PMMA) were utilized as shell and core, respectively. Nylon6 in the shape of pellets with the size of 3 mm, the density of 1.084 g/cm^3 at 25 °C and the molecular weight of 11202 g/mol was obtained from Sigma Aldrich (Ontario, Canada). PMMA with the average molecular weight of 120,000 was also supplied by Sigma. To prepare the polymeric solutions, formic acid with the purity of >98% (Sigma, Ontario, Canada) and Chloroform (Sigma, Ontario, Canada) were used as solvents for Nylon6 and PMMA, respectively. Ampicillin sodium salt (AC) used as a model drug was acquired from VWR International (Alberta, Canada). 0.2 micron filtered Methanol was also purchased from Fisher Scientific (Ontario, Canada) as a solvent for AC. For the purpose of preparing the Phosphate Buffer Solution (PBS), sodium phosphate in the granular shape and sodium vhloride (Purity≥99.5%) in the powder form were obtained from Fisher Scientific (Ontario, Canada) and Sigma (Ontario, Canada), respectively.

3.2. Methods

3.2.1. Instrumentation and optimization of the electrospinning setup[1]

Fig. 3-1 illustrates a schematic of an electrospinning setup capable of fabricating core/shell fibers. Based on this schematic, a coaxial electrospinning setup consists of: syringe pump, Dc high voltage generator, coaxial spinneret, grounded collector and tubing.
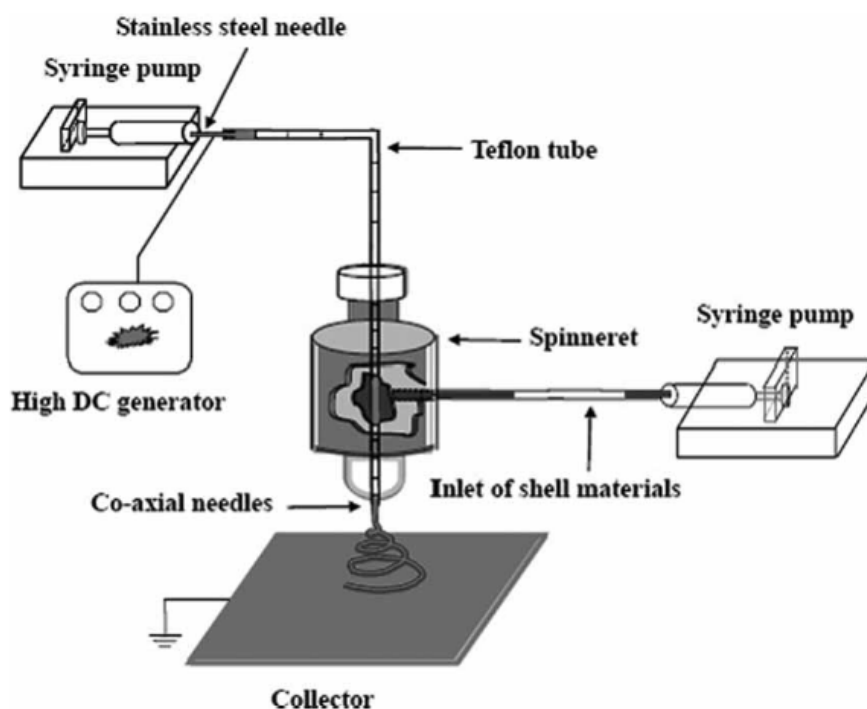
Fig. 3-1. Schematic of coaxial electrospinning setup [114].

In order to assemble a homemade electrospinning device, syringe pumps with the dispensing volume ranging from 10μl to 60ml and the pumping rate up to 426 ml/hr were purchased from Fisher Scientific (Ontario, Canada). Instead of using a conventional Ac-Dc high voltage generator, a 25A series Dc-Dc high voltage module was obtained from Ultravolt Inc. (NY, USA). The module is

42

capable of producing a high Dc voltage up to 25 kV with an input Dc voltage of 12 V and a power of 4watts. The module is able to produce a current of 0.19 mA. The polarity of the module used in this study is positive. The coaxial spinneret was supplied by Linari Engineering (Biomedical division, Piso, Italy). Fig. 3-2 clearly shows the structure of the coaxial spinneret. The internal needle has an inner diameter (ID) of 0.51 mm and an outer diameter (OD) of 0.83 mm. The ID and OD of the external needle are 1.37 and 1.83 mm, respectively.
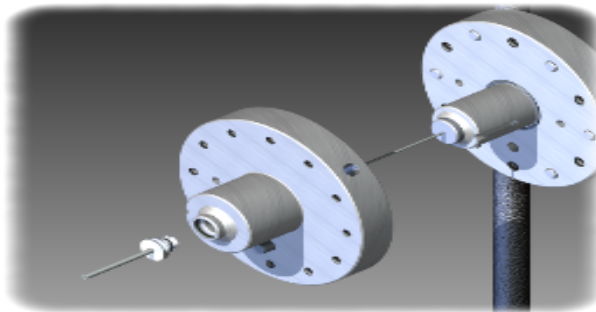
Fig. 3-2. The structure of the coaxial spinneret.

Fig. 3-3a shows the Dc-Dc high voltage module utilized in this study. Moreover, Fig. 3-3b illustrates the stainless steel box acting as a grounding shield. The different parts with their functionality indicated in the Fig. 3-3b are:

a)   b)
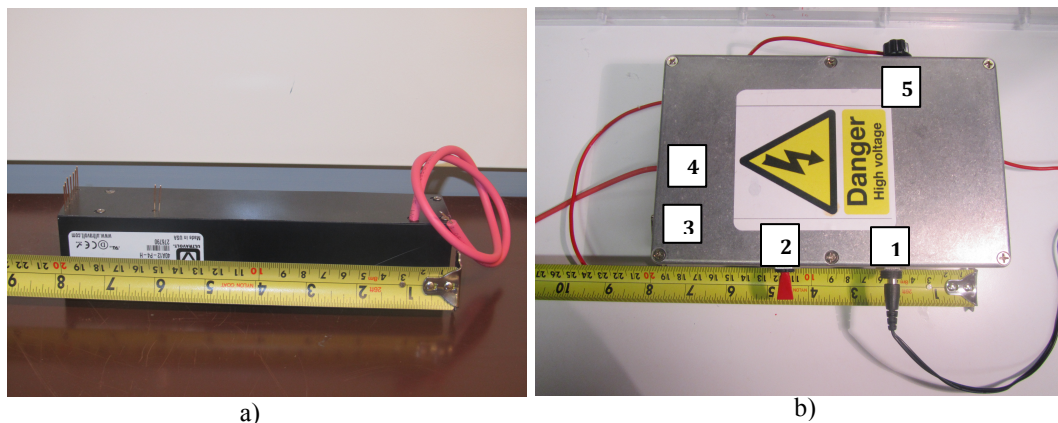
Fig. 3-3. a) The 25A series Dc-Dc high voltage module b) The grounding box labeled with different parts.

43

1- Input voltage of 12 V;

2- On/Off switch;

3- Grounding clip which is attached to the collector;

4- High voltage cable attached to the stainless steel needle in order to apply the high voltage to the polymeric solution and

5- Voltage adjustment knob which is able to increase the voltage up to 25kV.

Application of the Dc-Dc high voltage module instead of a conventional Ac-Dc high voltage supply has the advantage of decreasing the cost and increasing the mobility of the system. In order to shield the system from the surrounding environment to avoid possible arcing and electrocution, a shielding box was designed and prepared from Poly Acrylic sheets. Fig. 3-4a depicts a schematic of the above-mentioned shielding, whereas Fig. 3-4b shows an image

a)   b)
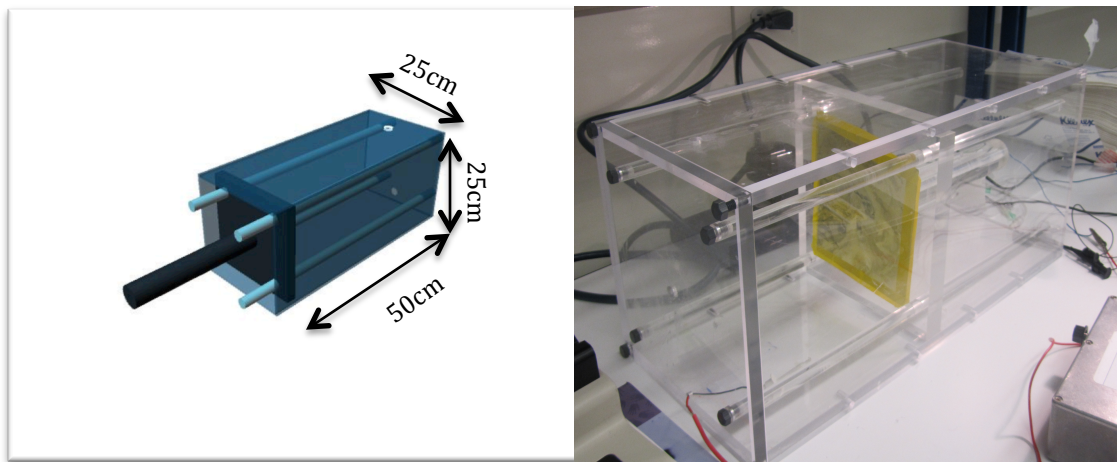
Fig. 3-4. a) The schematic of the electrospinning shielding b) The actual shielding used in the homemade setup.

of the actual shielding setup employed. Besides insulating the whole setup from the surrounding environment, a plunger located at the back of the shielding enables control over the distance between the collector and the nozzle.

As described in section 2.2, various parameters could affect the electrospinning process in terms of the diameter of the fibers and their overall size distribution. The most important parameters, which should be optimized in order to obtain fine fibers along with a narrow size distribution, are the applied voltage and the distance between the nozzle and the collector. In this study, optimization of the homemade electrospinning setup was carried out by varying the voltage and the distance while keeping other parameters such as the solution feeding rate, the polymer concentration and the temperature constant. All the experiments were performed at room temperature. Nylon6 solution with the concentration of 15 wt% was used as a model polymer. The solution was prepared by dissolving a sufficient amount of the Nylon6 pellets into formic acid and stirring magnetically until a homogenous transparent solution was obtained. The solution was transferred into a 5 ml plastic syringe with a gauge 21 needle (OD of 1.270 mm and ID of 0.838 mm). The solution feeding rate was kept constant at 0.3 ml/hr. The applied voltage and the distance varied in the range of 7.5-25 kV and 7.5-25 cm, respectively. The total number of 64 experiments carried out with afore-mentioned parameters. Scanning Electron Microscopy (SEM, VEGA-3, Tescan, USA) with the accelerating voltage of 20 kV was used to confirm the formation of the fibers, determine the diameter of the fibers and also evaluate the size

distribution. All samples were gold coated to avoid charging during SEM analysis (Denton Gold Sputter Unit).

3.2.2. Fabrication and characterization of the core/shell fibers

As illustrated in Fig. 3-2, a coaxial spinneret was utilized to produce core/shell fibers. Nylon6 with the concentration of the 15 wt% was prepared as mentioned in the previous section and used as the shell solution. Core solution consisted of two components. PMMA with the concentration of 15 wt% and Ampicillin sodium salt (AC) with various concentrations. The regular solvent for dissolving the PMMA powders is chloroform; however, since ampicillin is polar and it could not be dissolved in non-polar solvents such as chloroform, the combination of chloroform and methanol (9:1 v/v) was employed. The concentration of 15 wt% for PMMA was reached by adding an adequate amount of the PMMA powders to chloroform, which was stirred magnetically until a transparent solution was achieved. Different concentrations of ampicillin (1, 2, 5, 15 and 20 wt%) were first dissolved in sufficient amount of methanol and then, the whole mixture was added to the PMMA solution. The samples were named as NF-AC1, NF-AC2, NF-AC3, NF-AC4 and NF-AC5 with the drug concentrations of 1, 2, 5, 15 and 20 wt%, respectively. SEM was utilized in order to determine the diameter of the core/shell fibers. Moreover, the morphology of the fibers before and after the release of the encapsulated drug was examined using SEM as described in section 3.2.1. Transmission Electron Microscopy (TEM, Philips, Morgagni 268, USA) with the accelerating voltage of 80 kV was utilized in order to observe and confirm the formation of the core/shell fibers.

46

3.2.3. Characterization of the antibacterial drug

As previously stated, the model drug used in this study was ampicillin. The following sections explain the necessary characterizations that should be done prior to the in vitro drug release studies. It is worth mentioning that the in vitro drug release was done using Varian Carey 50 UV-Vis spectrophotometry (Agilent, USA). The first section discusses the method employed to prepare the media needed for all studies related to the characterization of the ampicillin and the rest of the sections describe the characterization techniques for the drug.

3.2.3.1. Preparation of the Phosphate Buffer Solution (PBS)

All the experiments involving the characterization of the drug or studying the drug release of the fibers were carried out in potassium buffer solution (PBS). In order to prepare the PBS, sodium phosphate and sodium chloride salts were dissolved in Milli-Q water with the concentration of 20 mM and 0.15 M, respectively. Afterwards, the pH of the whole solution was adjusted at 7.4 by using 0.1 M Hydrogen Chloride (HCl) solution.

3.2.3.2. Absorbance wavelength of ampicillin

The first step was to find the exact wavelength at which the absorbance of ampicillin molecules occurs. For this purpose, UV-Vis measurement utilized using two samples. The first sample used as a reference was pure PBS which is called blank sample and the second sample was PBS containing small amounts of ampicillin. All the measurements were performed at room temperature with scanning the wavelength in the range of 190-1000 nm.

3.2.3.3. Calibration curve

Results generated by UV-Vis spectroscopy are measured in absorbance; therefore, a tool is required to convert the absorbance to the concentration of the released drug (i.e. calibration curve). In order to acquire the calibration curve for AC, a series of solutions containing various concentrations of the AC (20,40,60,80 and 100 μg/ml) were prepared by means of serial dilution method. Afterwards, samples were analysed by means of UV-Vis spectroscopy and the resulted absorbance were plotted against the concentration. Based on the Beer-Lambert law, a linear relationship should be established between the concentration and the absorbance of the measured material. Hence, this linear relationship could be used in order to convert the absorption observed from UV-Vis spectroscopy to the concentration of the released drug.

3.2.4. In vitro drug release

The AC incorporated PMMA-Nylon6 core/shell fibrous mats were first cut into five small squares (1×1 cm^2) for each concentration of the incorporated drug, with the weights lying in the range of 11-13 mg for all the samples, and then immersed in 10 ml of PBS (pH7.4). All the samples were kept at 37 °C by means of unstirred water bath (VWR International, Alberta, Canada). At predetermined time intervals, 1 ml of the buffer solution from each sample was removed for further analysis. At the same time 1ml of fresh PBS was added to the remaining sample containers to continue the release. In vitro drug release studies were carried out using UV-Vis spectroscopy at the wavelength of 207 nm. The

acquired absorbance was then converted to the concentration by means of the calibration curve for AC.

3.2.5. Release kinetics and mechanisms studies

The drug release kinetics investigations for fabricated AC incorporated PMMA-Nylon6 core/shell fibers were carried out by means of the well know Korsmeyer-Peppas equation as described in section 2.3.2.1.

3.2.6. Diffusion coefficient calculations

As discussed by Koutsopoulos et al. the apparent diffusion coefficient of a polymeric matrix containing a well-dispersed diffusing agent could be calculated by means of 1D unsteady-state form of Fick's second law of diffusion [69], as below:

$$\frac{M_t}{M_\infty} = (\frac{16D_{app}t}{\pi H^2})^{0.5} \quad (3-1)$$

In which M_t and M_∞ are the concentration of the drug at desired time and the final concentration of the drug, respectively. "D_{app}" is the apparent diffusion coefficient of the system and "H" is the thickness of the fibers.

3.2.7. Biological activity measurements

Antibacterial activity of the AC incorporated core/shell fibers against *Listeria innocua* was monitored by measuring the optical density (OD) of the bacterial cultures using UV-Vis spectroscopy (DU 730 Life Science UV-Vis Spectrophotometer). In these studies, the measured OD was used to estimate the concentration of the bacteria. Twelve samples were prepared for this purpose as listed below. 5 samples of AC incorporated core/shell fibers with different AC

concentrations of 1%, 2%, 5%, 15%, and 20%. 5 samples were used as positive controls, which contain pure AC powders in 100 μl of distillated water with the concentrations relative to the concentrations of the released drug from NF-AC samples after 18 hours release which are denoted as AC1, AC2, AC3, AC4 and AC5. One sample was prepared by adding the AC-free fiber mats (NF) to the bacterial subculture. Finally, a blank sample was utilized by preparing the bacterial subculture with no fiberous mat in it (Blank). Initially, *L.innocua* was grown in 5ml tube of All-purpose tween (APT) medium overnight at 37$^{\text{o}}$c. Stock bacterial suspension (OD = 0.014) was then prepared by making serial dilution of the bacteria in the same media. 1ml of the stock bacteria suspension (OD = 0.014) was cultured independently with the samples and the blank in twelve sterile cuvettes. The subcultures were incubated at 37 $^{\text{o}}$C for 18 hours. The OD of samples after the incubation was measured with UV-Vis spectroscopy at 600 nm.

Chapter 4: Results and discussion

In the previous chapter, different experimental procedures involved in this study were discussed. In this chapter, acquired results are explained and discussions are carried out to justify the results.

4.1. Optimization of the electrospinning setup[1]

As stated previously, a series of 64 experiments were carried out with changing the applied voltage in the range of 7.5-25 kV and distance between the nozzle and the collector in the range of 7.5-25 cm in order to optimize the designed electrospinning setup in terms of the diameter and size distribution of the fabricated fibers. In this section, the aim is to investigate the effect of the electric field on the two aforementioned parameters. The electric field was varied in the range of 0-3.33 kV/cm by adjusting the applied voltage and the separation distance. After the electrospinning process, collectors containing the fibrous mats were removed and utilized for SEM analysis. Three different regimes of electric field were used:

I) E≤0.5 kV/cm

As discussed by Yang et al., one of the main requirements in an electrospinning process is sufficient electrostatic force in order to overcome the surface tension of the droplet formed at the tip of the nozzle [115]. The SEM images of collector material for electric field in this range showed no signs of fiber formation. This observation might be due to the fact that the electric field

[1] The results and discussions regarding the optimization of the setup presented in this section has been published in the Journal of Scanning Microscopies, DOI 10.1002/sca.21044.

were not sufficient to overcome the surface tension of the polymer droplet formed at the tip of the needle; therefore, a charged fluid jet could not be ejected towards the target.

II) 0.5<E<1 kV/cm

Fig. 4-1 illustrates the SEM images of the collector for two different voltage-distance ratios with the electric field lying in the above range. It could clearly be observed that the fibers were formed on the collector; however, the homogeneity of the fiber mat was compromised by the formation of belt-like entities, which are distinguishable from well-known cylindrical fibers.

a)   b)
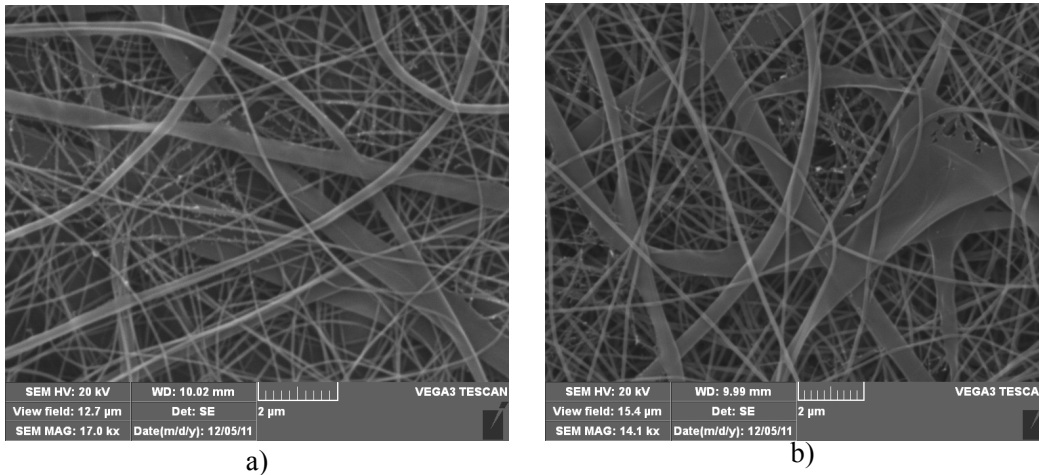
Fig. 4-1. The SEM images of different conditions with 0.5<E<1 kV/cm a) E=0.6 kV/cm b) E=0.8 kV/cm. Combined formation of nanofibers and belt like entities is a direct result of insufficient electrostatic forces due to low electric field (The scale of images is 2 μm).

The same line of reasoning that was used for the previous category could be applied in this range of electric field. At the present situation, although the electrostatic forces were high enough to produce fibers they were not sufficient to complete the transformation of the entire polymer solution, thus the formation of the belt-like entities was inevitable.

III) 1≤E≤3.33 kV/cm

As opposed to the conditions in I and II, a complete formation of the fibers could be realized in this range of electric field as illustrated in Fig. 4-2 Even though this electric field range shows the best results in terms of the fiber formation, it requires further investigation to discern the effect of the electric field on the diameter and the size distribution of the fibers more precisely. This can be achieved by dividing the entire range of this electric field regime into six subgroups of E=1, 1<E≤1.5, 1.5<E≤2, 2<E≤2.5, 2.5<E≤3 and 3<E≤3.33 kV/cm.
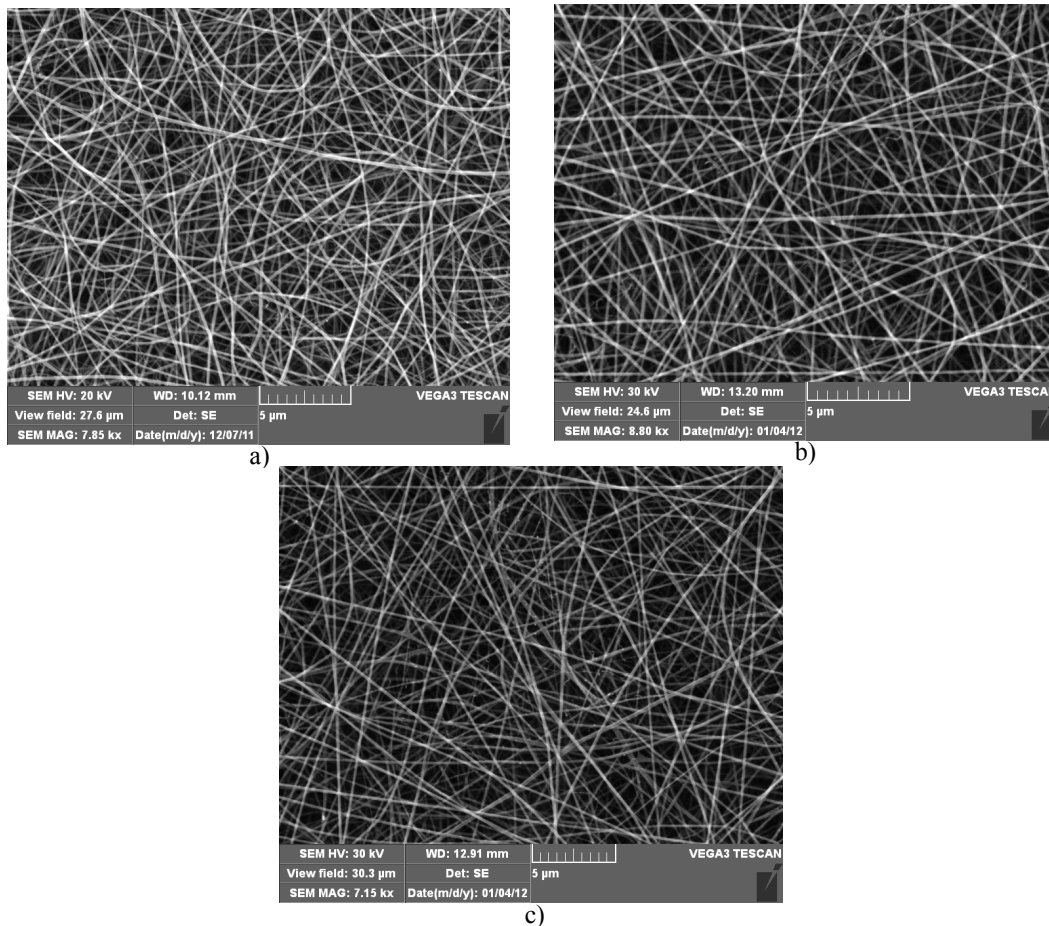
Fig. 4-2. The SEM images of different conditions with 1≤E≤3.33 kV/cm a) E=1 kV/cm b) E=2.6 kV/cm c) E=3.33 kV/cm. The complete formation of nanofibers is proven due to the absence of belt like entities (The scale in all images is 5 μm).

The effect of electric field could be studied from two points of view; i.e. the average fiber diameter and size distribution. Comparison between average fiber diameters calculated from the SEM images is shown in Fig. 4-3.
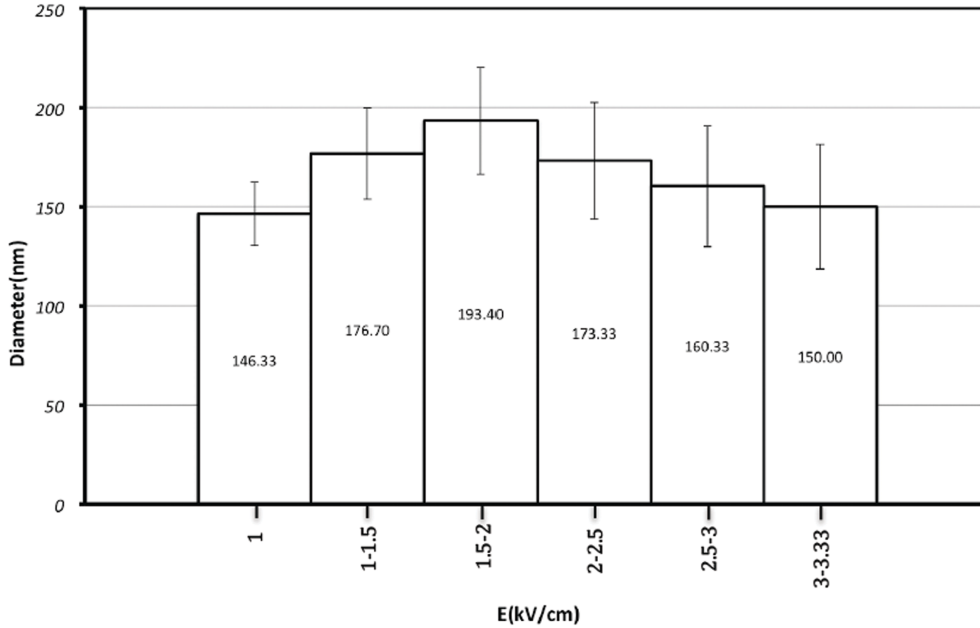
Fig. 4-3. The effect of six different electric field ranges lying in the span of $1 \leq E \leq 3.33$ kV/cm on the average diameter of the nanofibers. The increase in the electric field caused an initial increase in the average diameter due to the dominant effect of the number of bending instability cycles which followed by a decrease due to dominant effect of fiber thinning at higher electric field.

The size distribution of the fibers in each subgroup could be determined by means of standard deviation calculation. Table 4-1 summarizes the results of the standard deviation for each category. As the data in Fig. 4-3 suggests, the finest fiber diameter could be achieved by maintaining the electric field at 1 kV/cm as well as $3 < E \leq 3.33$ kV/cm; however, the standard deviation data in Table 4-1 indicates that the narrowest size distribution of fibers could be obtained at E=1 kV/cm.

Table 4-1. Standard deviation and average diameter of nanofibers with respect to the electric field.

E (kV/cm)	Diameter (nm)	Standard Deviation (nm)
1	146.33	16.00
1-1.5	176.7	23.00
1.5-2	193.4	27.60
2-2.5	173.33	30.00
2.5-3	160.33	29.82
3-3.5	150	31.00

Based on the observations of the Reneker et al. on the different steps of a bending instability cycle, discussed in section 2.1. [77], it could be hypothesized that the two important parameter which determine the diameter and the size distribution of the fibers are the fiber thinning due to the electrostatic forces and the number of bending instability cycles that the jet undergoes. The trend observed in Fig. 4-3 suggests that both parameters could affect the diameter and the size distribution of the fibers; however, it could be inferred that the average diameter is mostly controlled by the electrostatic forces and the size distribution is influenced mainly by the number of bending instability cycles. The entire trend could be explained based on this hypothesis that increasing the electric field causes the increase in the fiber thinning due to higher electrostatic forces; however, the number of bending instability cycles that the jet could undergo decreases. It has been established by Reneker et al. that bending instability will discontinue if the fiber solidification occurs [77]. Increasing the electric field results in the higher electrostatic forces which consequently causes the solvent to evaporate more quickly and the jet to solidify in less time. The initial increase in the fiber diameter is possibly due to the fact that the number of bending instability

cycles is decreasing; however, the effect of fiber thinning is so small that it is unable to compensate the lower number of the cycles. Afterwards, the fiber diameter decreases possibly as a consequence of the high fiber thinning ($2 < E \leq 3.3$) which could compensate for the low number of the bending instability cycles. The ascent in the standard deviation in Table 4-1 could be explained according to the above-mentioned hypothesis. Increasing the electric field eventually results in the lower number of the bending instability cycles and consequently the decrease in the diameter uniformity.

Since E=1 kV/cm could be reached with different combinations of voltage and distance, further investigation was performed on the diameter and the size distribution of fibers amongst all the combinations leading to this electric field. The average diameter and also the size distribution of the fibers in each of these combinations are compared in Fig. 4-4 and Table 4-2, respectively.
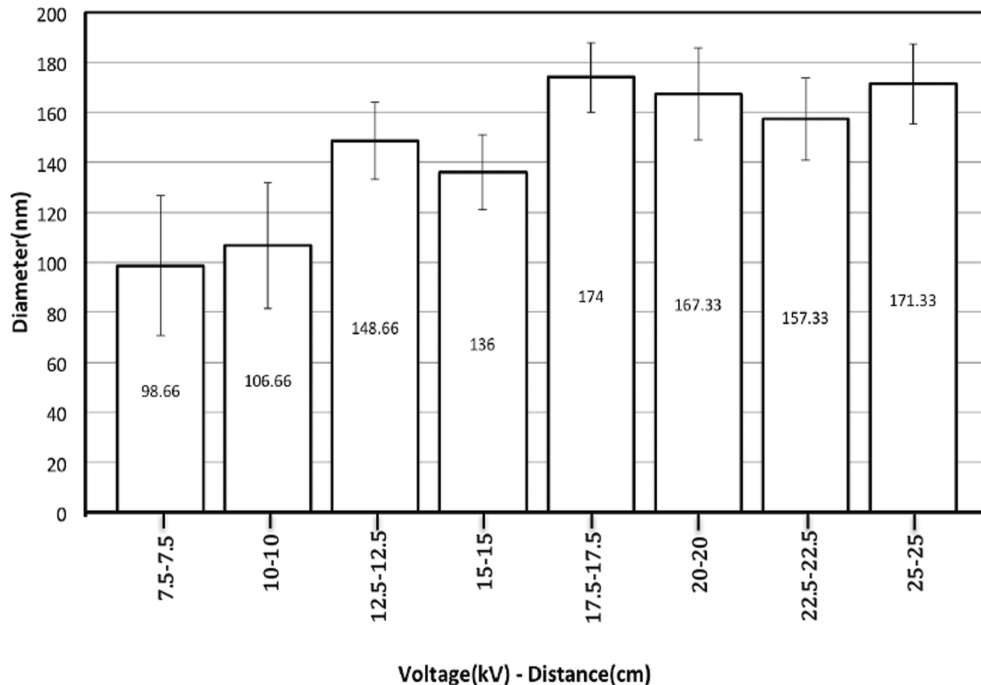
Fig. 4-4. The effect of different combinations of voltage and distance with the E=1 kV/cm on the average diameter of the nanofibers.

56

Considering the results in Fig. 4-4, although it could be concluded that the finest fibers could be achieved in the lowest voltage-distance combinations, i.e. 7.5 kV-7.5 cm and 10 kV-10 cm, the standard deviation results which were summarized in Table 4-2 suggest that these two combinations produce the widest size distributions amongst all combinations. Considering the fiber diameter and size distribution criteria, it could be inferred that the best combination in order to achieve fine fibers along with a narrow distribution is 15 kV-15 cm.

Table 4-2. Comparison between the standard deviation and average diameter of different voltage-distance combinations.

Combination	Diameter (nm)	Standard Deviation (nm)
7.5 kV-7.5 cm	98.66	27.99
10 kV-10 cm	106.66	25.26
12.5 kV-12.5 cm	148.66	15.52
15 kV-15 cm	136	15.02
17.5 kV-17.5 cm	174	14.04
20 kV-20 cm	167.33	15.8
22.5 kV-22.5 cm	157.33	16.67
25 kV-25 cm	171.33	15.97

Therefore, in order to prove this hypothesis, the size distributions of 7.5 kV-7.5 cm and 15 kV-15 cm combinations were studied by measuring the size of 100 fibers for each combination in SEM images. The size distribution of fibers at 7.5 kV-7.5 cm and 15 kV-15 cm are illustrated in Fig. 4-5a and Fig. 4-5b, respectively. It could be observed from Fig. 4-5a that the combination of 7.5 kV-

7.5 cm produces many different fiber diameters covering a range from 50 nm to 230 nm. However, Fig. 4-5b shows that the combination of 15 kV-15 cm generates a narrower size distribution comprising a range from 90 nm to 180 nm.
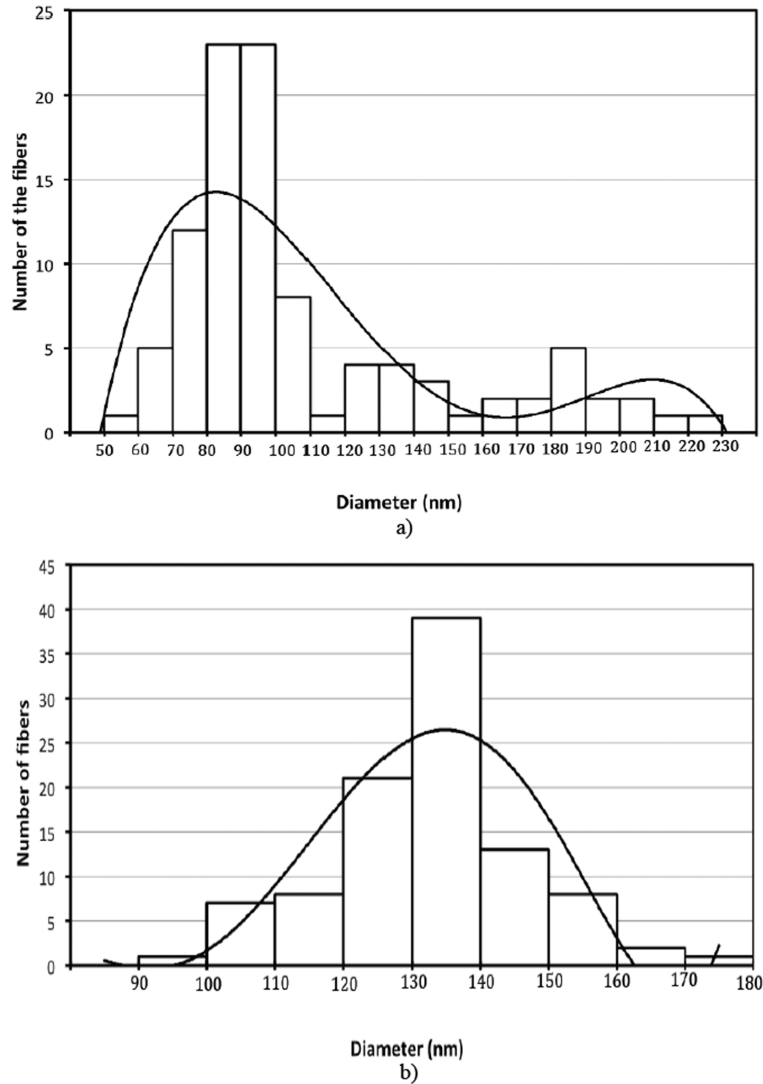
Fig. 4-5. The size distribution comparison between combinations a) 7.5 kV-7.5 cm and b) 15 kV-15 cm. Maintaining E=1 kV/cm with the combination of 15 kV-15 cm resulted in a more uniform size distribution of the fibers possibly due to the increased number of bending instability cycles as a result of the increased distance.

The same reasoning as above could be used in explaining the results. Increasing the distance between the two electrodes while maintaining the constant

electric field will possibly increase the numbers of the bending instability cycles since it allows increased time of flight for the jet. Thus, the combination of 15 kV-15 cm produces narrower size distribution.

4.2. Characterization of the core/shell fibers

Fig. 4-6 illustrates the SEM images of the core/shell fibers containing different contents of the encapsulated AC before the drug release process.
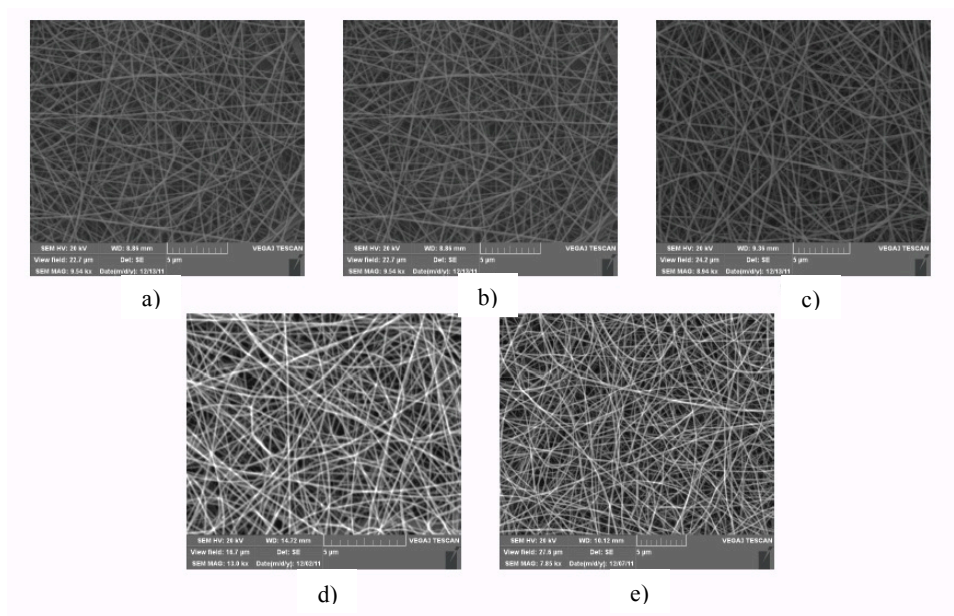
Fig. 4-6. The SEM images of the core/shell fibers before the drug release process a) NF-AC1 (1%), b) NF-AC2 (2%), c) NF-AC3 (5%), d) NF-AC4 (15%) and e) NF-AC5 (20%). All the images show the formation of the bead-free porous mats indicating the formation of the core/shell structure without deterioration of the morphology (The scale bars in all images are 5μm).

As illustrated in Fig. 4-6, bead-free continuous fibers formed as fibrous mats indicating that encapsulating the drug in the core did not deteriorate the morphology of the fibers. This is beneficial since deterioration in morphology of the fibers could affect the drug release behavior of the system significantly.
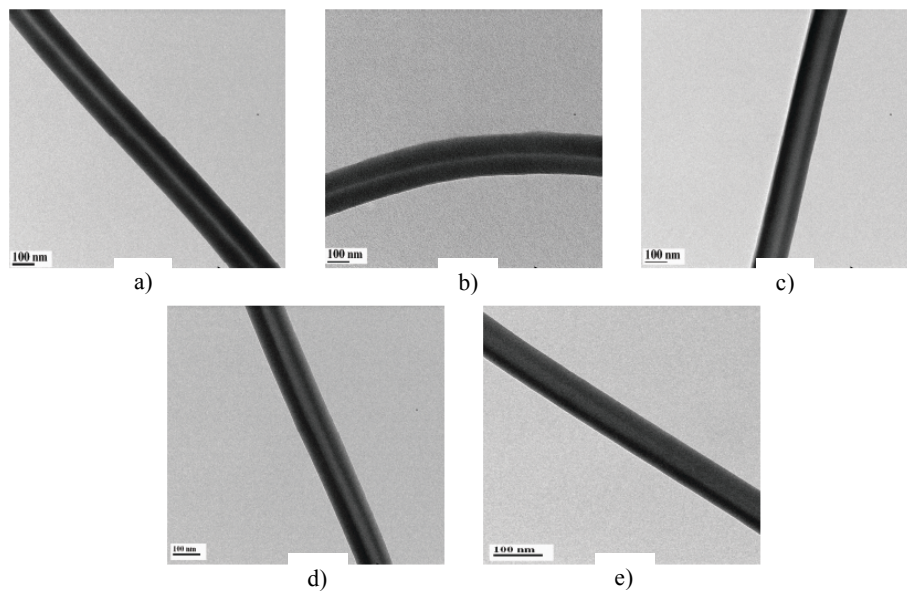
Fig. 4-7. The TEM images of the core/shell fibers a) NF-AC1 (1%), b) NF-AC2 (2%), c) NF-AC3 (5%), d) NF-AC4 (15%) and e) NF-AC5 (20%). The fabrication of the core/shell fibers are confirmed due to the sharp contrast formed between the core and the shell (The scale bars in all images are 100nm).

SEM analysis did not suffice to confirm the successful encapsulation of the AC in the fibers, ergo TEM analysis was utilized. Fig. 4-7 demonstrates the TEM images of the fibrous mats incorporated with various concentrations of AC. The formation of the fibers with a smooth surface could also be confirmed by TEM images shown in Fig. 4-7. More importantly, the sharp contrast at the vicinity of the core and shell for all concentrations of AC confirms the formation of the core/shell fibers. This could possibly be due to the immiscibility of the core and shell solutions; moreover, the fast processing of the electrospinning could prevent the mixture of the two solutions significantly [116]. The mean diameter of the fibers along with the average diameter of the core part of the fibers obtained from different concentrations of AC is summarized in Table 4-3.

Table 4-3. The average diameter for core segment and the overall diameter of the core/shell fibers with five different concentrations of the incorporated AC.

Ampicillin Concentration	1%	2%	5%	15%	20%
Core segment diameter (nm)	33	30	35	36	31
Whole fiber assembly diameter (nm)	166	160	140	126	94

The comparison between the diameters of the core segment of the fibers exhibits no significant change in the diameter as a result of the increase in the AC concentration; however, a noticeable gradual decrease in the diameter of the whole core/shell assembly is observed with the increase in the AC content. The ionic nature of the ampicillin sodium salt is believed to have the main contribution on the decrease of the fibers diameter. The effect of the ions in the solution on the charge build up at the tip of the needle during the electrospinning is a well-established fact. Increasing the AC content results in the increase of the numbers of the ions in the solution which subsequently causes the enhancement of the charge build up at the tip of the needle. This enhancement magnifies the effect of the electrostatic forces on the thinning of the fibers [117].

4.3. Drug characterization

As mentioned in chapter 3, the drug was characterized from two points of view i.e. the wavelength in which the absorbance of the drug occurs and the calibration curve for ampicillin sodium salt. Fig. 4-8 depicts the absorbance

wavelength and the calibration curve for AC, which were acquired based on the methods described in Sections 3.2.3.2 and 3.2.3.3, respectively.
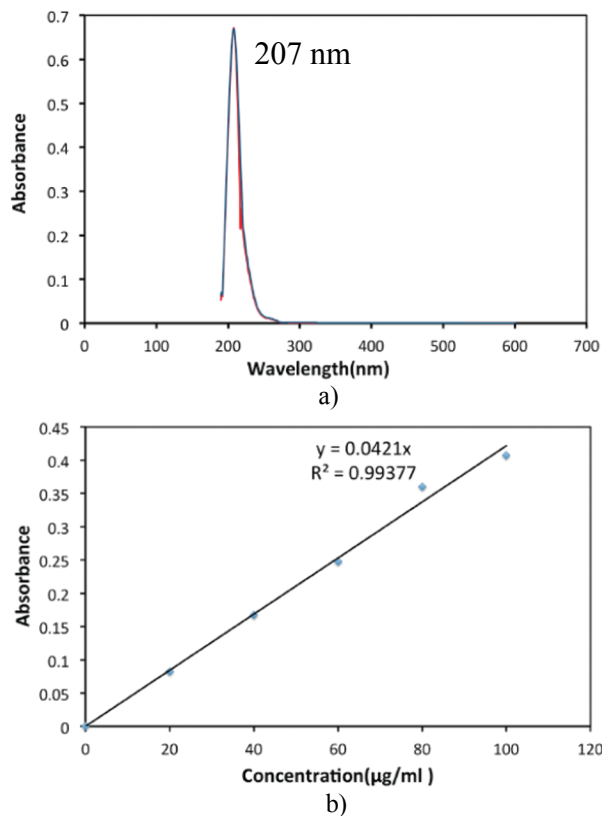
Fig. 4-8. a) The absorbance wavelength of the AC in the PBS media b) The calibration curve of AC.

As demonstrated in Fig. 4-8a, AC shows a sharp peak at 207 nm in the PBS (pH7.4) which could be used for further analysis in obtaining the calibration curve and also the drug release of the system. Fig. 4-8b illustrates the calibration curve obtained for AC in the PBS (pH7.4) media. A linear relationship between the absorbance and the concentration was expected based on the Beer-Lambert law. The obtained R-squared value confirms the feasibility of this calibration curve for this study. Therefore, Eq. 4-1 could be utilized to convert the absorbance values to the concentration values when the drug release study is considered.

$$Abs = 0.0421 \times concentration \quad (4-1)$$

4.4. In vitro drug release

The drug release behavior of the core/shell fibers with different concentrations of the drug inside the core is illustrated in Fig. 4-9. Three distinguishable stages could be observed for all the drug contents. The release of the drug underwent a burst release in stage I, which occurred during the first 6 hours of the release and it was responsible for approximately 30% of the release.
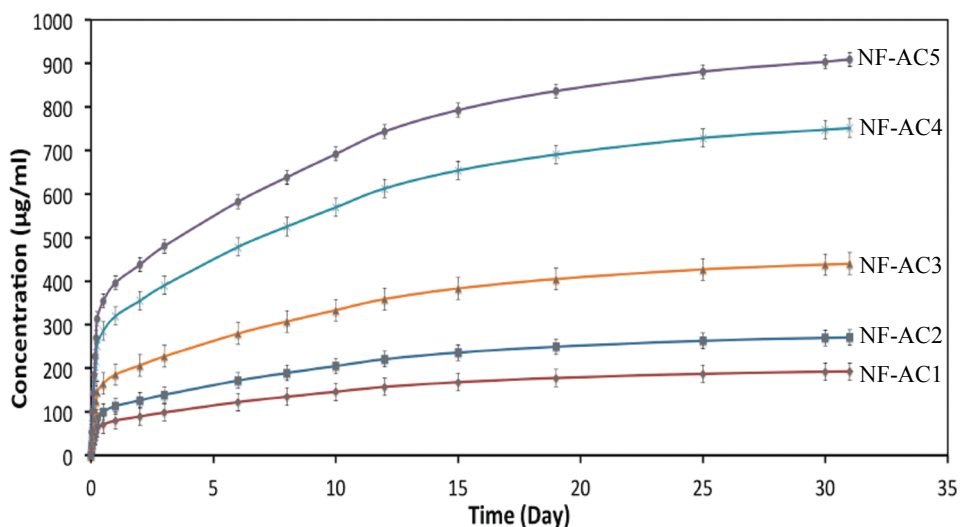
Fig. 4-9. The drug release behavior of the designed drug delivery systems with different concentrations of the encapsulated drug. All systems indicate a sustained drug release through three distinguishable stages over a period of 31 days.

The burst is most likely due to the combination of two simultaneous phenomena. (a) The accumulation of the drug molecules at or near the surface of the fibers during the electrospinning process, which consequently facilitates the release of the drug into the surrounding solution [69,118] along with, (b) the possible erosion of the surface of the fibers as a result of the incubation in the aqueous solution. This would allow drug molecules to escape the fibers much more simply through surface defects. The occurrence of this hypothesis will be

63

discussed in details by means of release kinetics calculations and SEM image of the fibers after the in vitro release process (section 4.5). Fig. 4-10 illustrates the burst release (stage I) of the drug from all the designed drug delivery systems. It could be inferred that although all the designed drug delivery systems exhibited the burst release, this stage was suppressed and occurred only in the first 6 hours of the release.
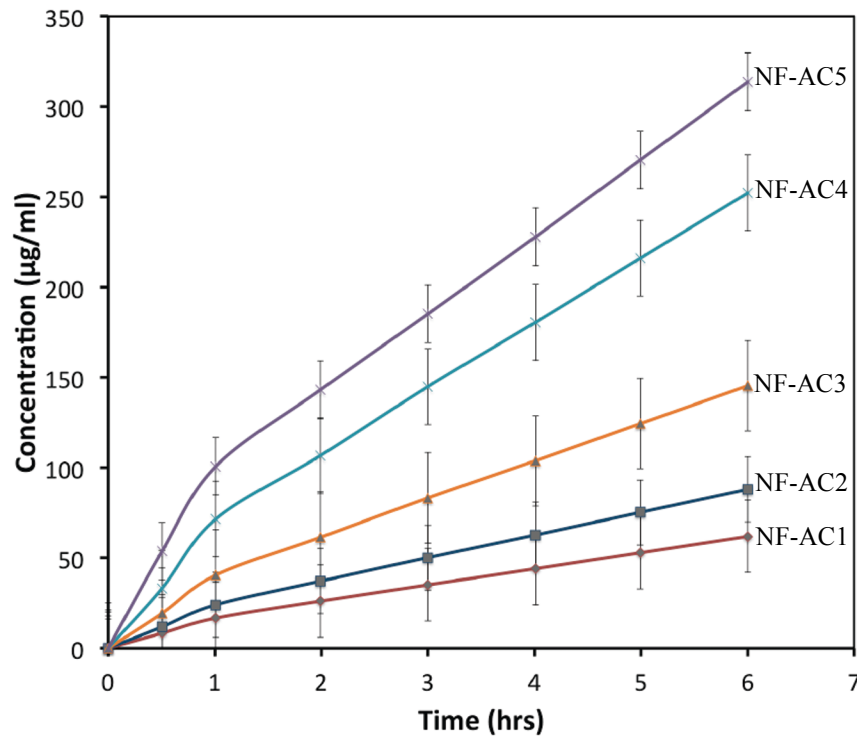
Fig. 4-10. The burst release (Stage I) of the AC from different systems. The burst release was suppressed to 6 hours by utilizing the core/shell fibers.

Stage II of the release for all the drug contents is comprised of a steady state drug release, in which almost 50% of the drug was released in 12 days. Finally, all five systems illustrated a gradual decrease in the release rate (stage III) until they reached their maximum release. It is believed that the main reason for this gradual decrease in the release rate is due to the fact that drug molecules are required to follow longer routes to escape the polymeric matrix. The results in Fig.

4-9 and Fig. 4-10 indicate that increasing the content of the drug incorporated into the core resulted in the higher concentration of the released drug at any given time interval. It could be hypothesized that, (a) increasing the concentration of the drug inside the core could possibly increase the drug concentration gradient between the fibrous mat and its surrounding environment. This would lead to an increase in the diffusion driving force. (b) Higher concentrations of the incorporated drug would magnify the accumulation of the drug molecules at or near the surface of the fibers during the electrospinning process that subsequently increases the release of the drug during the burst release (stage I) and (c) as discussed in [118,119], the release of the drug from a semi-crystalline polymeric matrix initially occurs from amorphous parts of the matrix. Moreover, increasing the amount of the drug in the polymeric fibers decreases the crystallinity of the polymeric carrier; therefore, the concentration of the drug released from the fibers increases. Regarding the results in this study, increasing the drug content in the core from 1% to 20% increased the concentration of the released drug significantly, which could be the consequence of the decreased crystallinity.

4.5. Kinetics and mechanisms of the drug release

Drug release kinetics could be studied utilizing the well-known Korsmeyer-Peppas equation. By converting Eq. 2-2 into a logarithm-based equation (Eq. 4-2), a linear relationship between Log ($\frac{M_t}{M_0}$) and Log (t) is expected for a release behavior that follows the Korsmeyer-Peppas release kinetics.

$$Log\left(\frac{M_t}{M_0}\right) = Log(k) + nLog(t) \qquad (4-2)$$

The slope of the line would be the release exponent (n), which could be used for the determination of the release mechanism. The results regarding the release kinetics studies of each release stage for different systems are summarized in Table 4-4. Firstly, R-squared values tabulated in Table 4-4 indicate that Korsmeyer-Peppas model used in this study fits the release data with close approximation; therefore, this model could be used for further analysis. As implied by Table 4-4, for all concentrations of the encapsulated AC, stage I of the release followed the non-Fickian diffusion. In other words, the release of the drug occurred through the combination of the diffusion from the polymeric matrix and the surface erosion of the fibers.

Table 4-4. Korsmeyer-Peppas parameters and the release mechanism for different systems at different stages.

Formulation		Release Stage	Model Parameters		Release Mechanism
Carrier formulation	AC contents(wt%)		n	R^2	
PMMA 15%(C)-Nylon6 15%(s)	1	I	0.78	0.9957	Non-Fickian diffusion
		II	0.25	0.9759	Fickian diffusion
		III	0.18	0.9878	Fickian diffusion
	2	I	0.78	0.9947	Non-Fickian diffusion
		II	0.24	0.9741	Fickian diffusion
		III	0.18	0.9902	Fickian diffusion
	5	I	0.78	0.9929	Non-Fickian diffusion
		II	0.24	0.9741	Fickian diffusion
		III	0.24	0.9761	Fickian diffusion
	15	I	0.78	0.9909	Non-Fickian diffusion
		II	0.24	0.9732	Fickian diffusion
		III	0.18	0.9925	Fickian diffusion
	20	I	0.68	0.9931	Non-Fickian diffusion
		II	0.23	0.9729	Fickian diffusion
		III	0.18	0.9929	Fickian diffusion

SEM analysis was utilized on NF-AC3 fibers (as the model sample) to observe the morphology of the fibers after the release process. Although the diameter of the fiber shown in Fig. 4-11 is larger than the diameter tabulated in Table 4-3, it was chosen since it clearly shows the surface morphology of the fiber after drug release. The formation of the cracks on the surface of the fiber is evidence of the proposed release mechanism for stage I, as illustrated in Fig. 4-11.
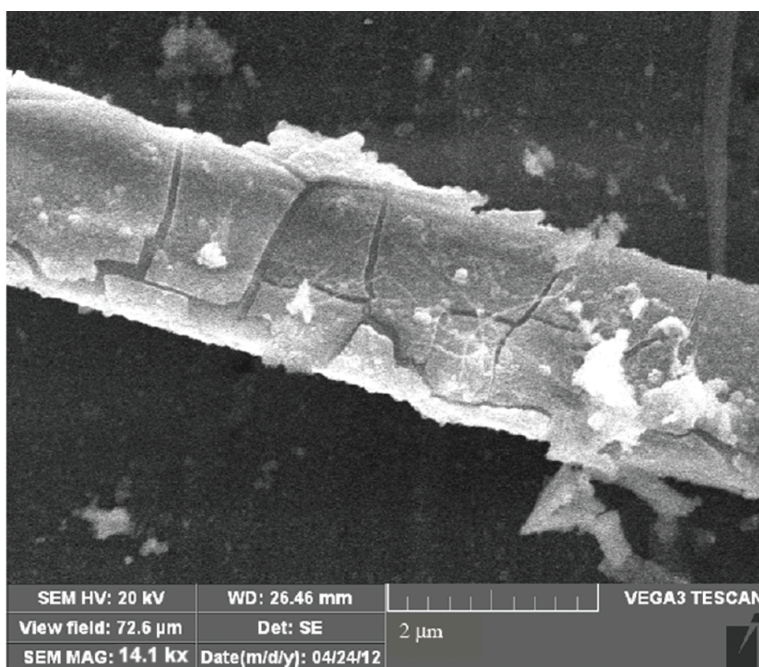
Fig. 4-11. The SEM image of the fiber after the drug release process (incubation at 37°C for 31 days). The formation of the cracks on the surface of the fiber evidenced the predicted mechanism of the non-Fickian diffusion (combination of diffusion and surface erosion) for the Stage I of the release.

It could be hypothesized that the occurrence of the non-Fickian diffusion in stage I could contribute to the burst release since it creates pathways (cracks on the surface) for drug molecules to release. As opposed to the proposed release mechanism for stage I, stages II and III underwent the Fickian diffusion in which the release of the drug molecules happened solely by diffusion.

4.6. Diffusion coefficient calculations

As stated before, Eq. 3-1 could be used to determine the apparent diffusion coefficient of a polymeric matrix containing a diffusing agent. Eq. 3-1 could be rearranged into Eq. 4-3 which indicates a linear correlation between $\frac{\pi H^2}{16} \times (\frac{M_t}{M_\infty})^2$ and $D_{app}t$.

$$\frac{\pi H^2}{16} \times (\frac{M_t}{M_\infty})^2 = D_{app}t \qquad (4-3)$$

Diffusion coefficients for different concentrations of the encapsulated AC were calculated for the stages that followed the diffusion mechanism (stage II and III) and summarized in Table 4-5.

Table 4-5. Diffusion coefficient calculations for stages that followed the Fickian diffusion mechanism (Stage II & III) for different contents of the incorporated drug.

Formulations		Release Stage	Model Parameters	
Carrier formulation	AC contents(wt%)		$D_{app} \times 10^{-21} (m^2/s)$	R^2
PMMA 15%(C)-Nylon6 15%(s)	1	II	6	0.9992
		III	0.7	0.9661
	2	II	3	0.9992
		III	0.7	0.9757
	5	II	2	0.9993
		III	0.5	0.9776
	15	II	1	0.9992
		III	0.4	0.9795
	20	II	1	0.9991
		III	0.3	0.9803

The R-squared values for all stages and concentrations of the drug indicate the feasibility of the utilized model for the drug release data. The most important point implied by Table 4-5 is the difference between the diffusion coefficient of the stage II and III for all the incorporated drug concentrations. The calculated diffusion coefficients for stage II are greater than that of calculated for stage III for all concentrations of the encapsulated drug. It could be hypothesized that increased crystallinity of the fibers as a consequence of the long-term incubation in the aqueous solution is possibly the main reason for the decrease in the diffusion coefficient from stage II to stage III. It has been established previously that the long-term incubation of fibers could cause the increase in the crystallinity and the diffusion of the small molecules from a crystalline segment of a polymeric matrix is slower than from amorphous parts [120,121].

4.7. Antibacterial activity of the core/shell fibers

The antibacterial activity of the AC incorporated core/shell fibers investigated through the optical density (OD) method is illustrated in Fig. 4-12. The results indicate that the growth of the bacteria occurred completely in the sample in which no fibrous mat existed, denoted by Blank in Fig. 4-12. Furthermore; the decrease in the OD, which indicates the decrease in the concentration of the bacteria, is insignificant for the fibrous mat with no drug encapsulation (NF), implying that the PMMA-Nylon6 core/shell nanofibers did not indicate any antibacterial activity by itself. The OD of the fibrous mats containing 1%, 2%, 5%, 15% and 20% of the AC indicated by NF-AC1, NF-AC2, NF-AC3, NF-AC4 and NF-AC5 in Fig. 4-12, respectively, shows a gradual

70

decrease with a significant drop at NF-AC3 (5%). Increasing the concentration of the encapsulated drug resulted in the higher concentration of the released drug after 18hrs as implied by Fig. 4-9, which consequently caused the higher degree of growth inhibition. In addition, the significant decrease in OD at NF-AC3 could be explained in the following manner; the concentration of the released drug from NF-AC3 was sufficient to inhibit the growth of the utilized concentration of the bacteria, subsequently no significant change in the OD was observed from NF-AC3 to NF-AC5 (20%).
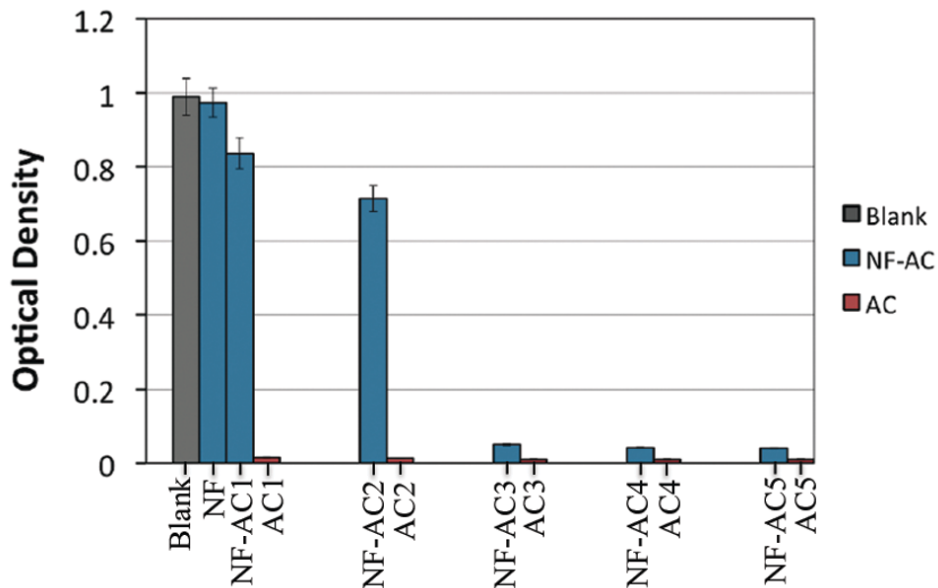
Fig. 4-12. Antibacterial activity of the core/shell nanofibers loaded with AC investigated by OD measurement. The gradual decrease of OD for NF-AC1, NF-AC2, NF-AC3, NF-AC4 and NF-AC5 which correspond to 1%, 2%, 5%, 15% and 20% of the encapsulated drug, respectively, indicates the higher effectiveness of fibers containing higher drug contents. Low optical density for positive control samples indicated by AC1 to AC5 implies the fact that adding the drug powder in the initial stage (t=0) could eliminate all the initial bacteria before incubation; therefore, no growth was observed

The amount of OD for positive control samples indicated by AC1 (1%), AC2 (2%), AC3 (5%), AC4 (15%) and AC5 (20%) in Fig. 4-12 showed a significant decrease regardless of the amount of the drug powder used as positive controls. It

could be hypothesized that introducing the final concentration of the drug which would be released after 18 hours from the fibers at the initial stage of the incubation (t=0) could possibly eliminate all the bacteria; therefore no growth of bacteria occurred in the incubation process.

Chapter 5: Conclusion and future work[1]

Producing nanofibers with controllable diameter and narrow size distribution is very important in many practical applications. The effect of electric field and distance-voltage combination on the average diameter and size distribution of the nanofibers of Nylon6 fabricated at room temperature by means of electrospinning of Nylon6 solution was investigated. SEM analysis of the electrospun fibers and diameter calculations indicated that the most proper electric field to obtain the finest fibers with the narrowest size distribution is E=1 kV/cm. We have found that even though maintaining the electric field at 1 kV/cm with a potential-distance combination of 7.5 kV-7.5 cm could result in the fabrication of the finest fibers, this voltage-distance combination resulted in a broad size distribution. A voltage-distance ratio of 15 kV-15 cm resulted in a narrow size distribution, although the average diameter was slightly larger than that obtained at 7.5 kV-7.5 cm combination.

In the second part of the study, ampicillin incorporated PMMA-Nylon6 core/shell fibers were fabricated utilizing the coaxial electrospinning technique. The formation of the core/shell structure and the continuous fibers with bead-free morphology were confirmed by means of TEM and SEM analysis, respectively. A gradual decrease in the overall diameter of the fibers was observed by increasing the content of the encapsulated drug from 1% to 20% possibly due to the increase in the conductivity of the electrospinning solution as a consequence of the ionic nature of the ampicillin sodium salt. The designed drug delivery system for all the

concentrations of the encapsulated drug indicated a three stages drug release over a period of 31 days with a sustained manner and suppressed burst release, which occurred only for 6 hours. The release kinetics and mechanisms investigations implied that the first stage for all the contents of the incorporated drug followed the non-Fickian diffusion i.e. the combination of the diffusion from fibers and the surface erosion of the fibers which was confirmed by SEM analysis of the fibers after the release process; however, stages II and III obeyed the Fickian diffusion. The diffusion coefficient calculations for the stages that followed the Fickian diffusion indicated lower coefficients for stage III comparing to the stage II for all the drug concentrations which is believed to be due to the crystallization of the fibers as a consequence of the long-term incubation at 37 °C in the aqueous solution. Antibacterial investigations showed a gradual decrease in the OD (concentration of the bacteria) by increasing the concentration of the encapsulated drug from 1% to 20%. In other words, increasing the contents of the encapsulated drug increased the concentration of the released drug after 18 hours incubation that resulted in the higher degree of the growth inhibition.

In order to take the investigation one step further, we would like to propose the incorporation of the nanoplates in fibers. The antibacterial properties of the fibers containing various nanoparticles such as silver nanoparticles have been established previously; however, the incorporation of the nanoplates in the fibers, especially in the core/shell structure has not been studied extensively. We have conducted a preliminary study on the incorporation of the $Mg(OH)_2$ nanoplates into Nylon6 nanofibers in terms of TEM analysis. The results

indicated that the orientation of the nanoplates (edge-wise or surface-wise) in the fibers could be controlled by adjusting the concentration of the nanoplates in the initial solution; however, more investigations are required to confirm these observations. The idea is to incorporate a drug in the core and embed $Mg(OH)_2$ nanoplates in the shell of the core/shell structure. In this way, the release of the drug from the core along with the higher chance of the existence of the nanoplates on the surface of the fibers as a result of the core/shell structure (comparing to a normal fibers) could enhance the antibacterial activity of the fibers.

Bibliography

[1] A, Ziabicki, Fundamentals of fiber formation, John Wiley and Sons (1976) ISBN 0-471-98220-2.

[2] G. M. Bose, Recherches sur la cause et sur la veritable theorie de la electricite. Wittenberg (1745).

[3] Lord Rayleigh, On the equilibrium of liquid conducting masses charged with electricity, Philos. Mag. 14 (1882) 184-186.

[4] J. F. Cooley, US 692631, Apparatus for electrically dispersing fluids (1902).

[5] W. J. Morton, US 705691, Method of dispersing fluids (1902).

[6] J. F. Cooley, US 745276, Electrical method of dispersing fluids (1903).

[7] K. Hagiwaba, O. Oji-Machi, K. Ku, Jpn 1699615, Process for manufacturing artificial silk and other filaments by applying electric current (1929).

[8] A. Formhals, US 1975504, Process and apparatus for preparing artificial threads (1934).

[9] M. Jacobsen, Chemiefasern/Textilind (1991) 36-41.

[10] J. Doshi, G. Srinivasan, D. Reneker, High Modulus Polymers: A Novel Electrospinning Process, Polymer News 20 (1995) 206-207.

[11] A. Greiner, J. H. Wendorff, Electrospinning: A Fascinating Method for the Preparation of Ultrathin Fibers, Angew. Chem. Int. 46 (2007) 5670-5703.

[12] S. Agarwal, J. Wendorff, A. Greiner, Use of electrospinning technique for biomedical applications, Polymers 49 (2008) 5603-5621.

[13] G. Taylor, Disintegration of water drops in an electric field, Proc. R. Soc. Lond. 280(A) (1964) 383-397.

[14] S. N. Reznik, A. L. Yarin, A. Theron, E. Zussman, Transient and steady shapes of droplets attached to a surface in a strong electric field, J. Fluid. Mech. 516 (2004) 349-377.

[15] M. Cloupeau, B. Prunet-Foch, Electrostatic spraying of liquids in cone-jet mode, J. Electrostat. 22 (1989) 135-159.

[16] A. L. Yarin, S. Koombhongse, D. H. Reneker, Taylor cone and jetting from liquid droplets in electrospinning of nanofibers, J. Appl. Phys. 90 (2001) 4836-4846.

[17] J. Lyons, C. Li, F. Ko, Melt-electrospinning part I: processing parameters and geometric properties Polymers 45 (2004) 7597-7603.

[18] P. D. Dalton, K. Klinkhammer, J. Salber, D. Klee, M. Msller, Direct In vitro electrospinning with polymer melts, Biomacromolecules 7 (2006) 686-690.

[19] R. Rangkupan, D. H. Reneker, Electrospinning process of molten polypropylene in vacuum J. Met. Mater. Miner. 12 (2003) 81-87.

[20] B. Ding, E. Kimura, T. Sato, S. Fujita, S. Shiratori, Polymer 45 (2004) 1895-1900.

[21] W. Tomaszewski, M. Szadkowski, Investigation of Electrospinning with the Use of a Multi-jet Electrospinning Head, Fibers & Textiles in Eastern Europe 13(52) (2005).

[22] Y. Z. Zhang, X. Wang, Y. Feng, J. Li, C. T. Lim, S. Ramakrishna, Coaxial Electrospinning of (Fluorescein Isothiocyanate-Conjugated Bovine Serum Albumin)-Encapsulated Poly (E-caprolactone) Nanofibers for Sustained Release, Biomacromolecules 7 (2006) 1049-1057.

[23] Filatov, Y. Budyka, A. Kirichenko, V. (Trans. D. Letterman), Electrospinning of micro- and nanofibers: fundamentals and applications in separation and filtration processes, Begell House Inc., New York, USA (2007) ISBN 978-1-56700-241-6.

[24] V. Thavasi, G. Singh, S. Ramakrishna Electrospun nanofibres in energy and environmental applications: Tools and Resources. Energ. Environ. Sci. 1 (2008) 205-221.

[25] T. H. Grafe, M. Gogins, M. A. Barris, J. Schaefer, R. Canepa, Nanofibers in Filtration Applications in Transportation, Filtration International Conference and Exposition, Chicago, USA (2001).

[26] J. C. Mycock, J. C. McKenna, L. Theodore, Fabric Filters, Handbook of Air Pollution Control Engineering and Technology, CRC Press Inc., Boca Raton, USA (1995).

[27] D. Bjorge, N. Daels, S. De Vrieze., P. Dejans, T. Van Camp., W. Audenaert, P. Westbroek., K. De Clerck., C. Boeckaert, S.W. van Hulle, Initial testing of electrospun nanofibre filters in water filtration applications, Water SA 36(1) (2010).

[28] F. Dotti, A. V. Aresano, A. M. Ontarsolo, A. A. Luigi, C. T. Onin, G. M. Azzuchetti, Electrospun Porous Mats for High Efficiency Filtration, J. Ind. Textil. 37 (2007).

[29] S. Malato, P. Fernandez-Ibanez, M.I. Maldonado, J. Blanco, W. Gernjak,

Decontamination and disinfection of water by solar photocatalysis: recent overview and trends, Catal. Today 147 (2009) 1-59.

[30] R.J. Braham, A.T. Harris, Review of major design and scale-up considerations for solar photocatalytic reactors, Ind. Eng. Chem. Res. 48 (2009) 8890-8905.

[31] M.N. Chong, B. Jin, C.W.K. Chow, C. Saint, Recent developments in water treatment technology: A review, Water Res. 44 (2010) 2997-3027.

[32] G. Laera, B. Jin, H. Zhu, A. Lopez, Photocatalytic activity of TiO2 nanofibers in simulated and real municipal effluents, Catal. Today 161 (2011) 147–152.

[33] J. Kong, N. Franklin, C. Zhou, M. Chapline, S. Peng, K. Cho, H. Dai, Nanotube molecular wires as chemical sensors, Science 287 (2000) 622-625.

[34] W. Gopel, K. Schierbaum, SnO_2 sensors current status and future prospects, Sens. Actuat. B-Chem. 26 (1995) 1-12.

[35] Y. Yamada, Y. Seno, Y. Masuoka, K. Yamashita, Nitrogen oxides sensing characteristics of Zn_2SnO_4 thin film, Sens. Actuat. B-Chem. 49 (1998) 248-252.

[36] J. Slater, E. Watt, N. Freeman, I. May, D. Weir, Gas and vapor detection with poly(pyrrole) gas sensors, Analyst 117 (1992) 1265-1270.

[37] J. Slater, J. Paynter, E. Watt, Multilayer conducting polymer gas sensor arrays for olfactory sensing, Analyst 118 (1993) 379-384.

[38] K. Schierbaum, U. Weimar, W. Gopel, Comparison of ceramic, thick-film and thin-film chemical sensors based upon SnO_2, Sens. Actuat. B-Chem. 7 (1992) 709-716.

[39] N. Savage, B. Chwierogh, A. Ginwalla, B. Patton, S. Akbar, P. Dutta, Composite n-p semiconducting titanium oxides as gas sensors, Sens. Actuat. B-Chem. 79 (2001) 17-27.

[40] M. Lonergan, E. Severin, B. Doleman, S. Beaber, R. Grubb, N. Lewis, Array-based vapor sensing using chemically sensitive, carbon black-polymer resistor, Chem. Mater. 8 (1996) 2298-2312.

[41] S. Unde, J. Ganu, S. Radhakrishnan, Conducting polymer-based chemical sensor: characteristics and evaluation of polyaniline composite films, Adv. Funct. Mater. 6 (1996) 151-157.

[42] W. Gopel, Supramolecular and polymeric structures for gas sensors, Sens. Actuat. B-Chem. 24 (1995) 17-32.

[43] D. Lee, S. Han, J. Huh, D. Lee, Nitrogen oxides-sensing characteristics of WO_3-based nanocrystalline thick film gas sensor, Sens. Actuat. B-Chem. 60 (1999) 57-63.

[44] B. Ding, M. Wang, J. Yu, G. Sun, Gas Sensors Based on Electrospun Nanofibers. Sensors 9 (2009) 1609-1624.

[45] V. Syritski, J. Reut, A. Opik, K. Idla, Environmental QCM sensors coated with polypyrrole Synthetic Meth. 102 (1999) 1326-1327.

[46] B. Ding, J. Kim, Y. Miyazaki, S. Shiratori, Electrospun nanofibrous membranes coated quartz crystal microbalance as gas sensor for NH_3 detection, Sens. Actuat. B-Chem. 101 (2004) 373-380.

[47] S. Wei, M. Zhoua, W. Du, Improved acetone sensing properties of ZnO hollow nanofibers by single capillary electrospinning, Sens. Actuat. B-Chem. 160 (2011) 753- 759.

[48] R. Vasita, D. Katti, Nanofibers and their applications in tissue engineering, Int J Nanomedicine 1(1) (2006) 15-30.

[49] G. K. Sangamesh, P. N. Syam, J. Roshan, M. V. Hogan, C. T. Laurencin, Recent Patents, Biomed Eng 1 (2008) 68-78.

[50] S. Agarwal, J. H. Wendorff, A. Greiner, Use of electrospinning technique for biomedical applications, Polymer 49 (2008) 5603-5621.

[51] M. M. Stevens, J. H, George, Science 310 (2005) 1135-8.

[52] D. N. Rockwood, K. A. Woodhouse, J. D. Fromstein, D. B. Chase, J. F. Rabolt, J. Biomater. Sci. Polym. 18(6) (2007) 743-58.

[53] P. Carampin, M. T. Conconi, S. Lora, A. M. Menti, S. Baiguera, S. Bellini et al., J. Biomed. Mater. Res. 80A(3) (2007) 661-8.

[54] J. Zhang, H. Qi, P. Hu, S. Guo, J. Li, Y. Che et al., Artif. Organs. 30(12) (2006) 898-905.

[55] H. A. Jerome, M. Simonet, A. Pandit, P. Neuenschwander, J. Biomed. Mater. Res. 82A(3) (2007) 669-79.

[56] O. D. Schneider, S. Loher, T. J. Brunner, L. Uebersax, M. Simonet, R. N. Grass et al., J. Biomed. Mater. Res. 84B(2) (2008) 350-62.

[57] A. Sui, X. Yang, F. Mei, X. Hu, G. Chen, X. L. Deng et al., J. Biomed. Mater. Res. 82A(2) (2007) 445-54.

[58] L. Chunmei, C. Vepari, H. Jin, H. Kim, D. Kaplan, Electrospun silk-BMP-2

scaffolds for bone tissue engineering, Biomaterials 27(16) (2006) 3115-3124.

[59] K. L. Kilpadi, P. L. Chang, S. L. Bellis, Hydroxylapatite binds more serum proteins, purified integrins, and osteoblast precursor cells than titanium or steel. J. Biomed. Mater. Res. 57(2) 2001 258-67.

[60] M. Goldberg, R. Langer, X. Jia. J. Biomater. Sci. Polym. 18(3) (2007) 241-68.

[61] X. Xu, X. Chen, P. Ma, X. Wang, X. Jing, The release behavior of doxorubicin hydrochloride from medicated fibers prepared by emulsion-electrospinning, Eur. J. Pharm. Biopharm. 70 (2008) 165-170.

[62] J.R.B.J. Brouwers, Advanced and controlled drug delivery systems in clinical disease management, Pharm. World Sci. 18 (1996) 153-162.

[63] X.H. Zong, K. Kim, C. Benjamin, Structure and process relationship of electrospun bioabsorbable nanofiber membranes, Polymer 43 (2002) 4403-4412.

[64] Y.H. Bae, K.M. Huh, Y. Kim, K.H. Park, Biodegradable amphiphilic multiblock copolymers and their implications for biomedical applications, J. Control. Release 64 (2000) 3-13.

[65] M. Miyajima, A. Kiko, J. Okada, M. Ikeda, Mechanism of drug release from poly (L-lactic acid) matrix containing acidic or neutral drugs, J. Control. Release 60 (1999) 199-209.

[66] E.R. Kenawy, G.L. Bowlin, G.E. Wnek, Release of tetracycline hydrochloride from electrospun poly (ethylene-co-vinylacetate), poly (lactic acid) and a blend, J. Control. Release 81 (2002) 57-64.

[67] S. Freiberg, X.X. Zhu, Polymer microsphere for controlled drug release, Int. J. Pharm. 282 (2004) 1-18.

[68] C.B. Packhaeuser, J. Schnieders, C.G. Oster, T. Kissel, In situ forming parenteral drug delivery systems: an overview, Eur. J. Pharm. Biopharm. 58 (2004) 445–455.

[69] Koutsopoulos, Sotirios et al., Controlled release of functional proteins through designer self-assembling peptide nanofiber hydrogel scaffold, Proc. Natl. Acad. Sci. 106(12) (2009) 4623-4628.

[70] B. Swaminathan, P. Gerner-Smidt, The epidemiology of human Listeriosis, Microbes Infect. 9 (2007) 1236.

[71] F. Allerberger, M. Wagner, Listeriosis: a resurgent foodborne infection, Clin. Microbiol. Infect. 16 (2010) 16.

[72] S. Bredholt, J. Maukonen, K. Kujanpaa, T. Alanko, U. Olofson, U. Husmark, A.M. Sjoberg, G. Wirtanen, Microbial methods for assessment of cleaning and disinfection of food-processing surfaces cleaned in a low-pressure system, Eur. Food Res. Technol. 209 (1999) 145-152.

[73] J. F. de la Mora, The Fluid Dynamics of Taylor Cones, Annu. Rev. Fluid Mech. 39 (2007) 217-243

[74] S. Agarwal, J. Wendorff, A. Greiner, Use of electrospinning technique for biomedical applications, Polymer 49 (2008) 5603–5621.

[75] P. K. Baumgarten, J. Colloid Interface Sci. 36 (1971) 71.

[76] S. B. Warner, A. Buer, S. C. Ugbolue, B. C. Rutledge, M. Y. Shin, National Textile Center Annual Report No. 83-90 (1998).

[77] D. H. Reneker, A. L. Yarin, H. Fong, S. Koombhongse, Bending instability of electrically charged liquid jets of polymer solutions in electrospinning, J. Appl. Phys. 87(9) (2000) 4531-4547.

[78] M. M. Hohman, M. Shin, G. Rutledge, M. P. Brenner, Electrospinning and electrically forced jets. I. Stability theory, Phys. Fluids 13 (2001) 2201-20.

[79] M. M. Hohman, M. Shin, G. Rutledge, M. P. Brenner, Electrospinning and electrically forced jets. II. Applications, Phys. Fluids 13 (2001) 2221-36.

[80] A. L. Yarin, S. Koombhongse, D. H. Reneker, Taylor cone and jetting from liquid droplets in electrospinning of nanofibers, J. Appl. Phys. 90 (2001) 4836-46.

[81] D. H. Reneker, A. L. Yarin, E. Zussman, H. Xu, Electrospinning of nanofibers from polymer solutions and melts, ADV. APPL. MECH. 41 (2007) 143-195.

[82] S. A. Theron, A. L. Yarin, E. Zussman, E. Kroll, Multiple jets in electrospinning: experiment and modeling, Polymer 46 (2005) 2889-99.

[83] J. J. Feng, Stretching of a straight electrically charged viscoelastic jet, J. Non newton. Fluid. Mech. 116 (2003) 55-70.

[84] C. J. Thompson, G. G. Chase, A. L. Yarin, D. H. Reneker, Effects of parameters on nanofiber diameter determined from electrospinning model, Polymer 48 (2007) 6913-6922.

[85] V. Beachley, W. Xuejun ,Effect of electrospinning parameters on the nanofiber diameter and length, Mater Sci Eng C 29 (2009) 663-668.

[86] S-H. Tan, R. Inai, M. Kotaki, S. Ramakrishna, Systematic parameter study for ultra-fine fiber fabrication via electrospinning process, Polymer 46(16) (2005)

6128-6134.

[87] X.M. Mo, C.Y. Xu, M. Kotaki, S. Ramakrishna, Biomaterials 25 (2004) 1883-1890.

[88] M.M. Demir, I. Yilgor, E. Yilgor, B. Erman, Polymer 43 (2002) 3303-3309.

[89] D.S. Katti, W. Kyle, K.W. Robinson, F.K. Ko, C.T. Laurencin, J. Biomed. Mater. Res. B: Appl. Biomater. 70B (2004) 286-296.

[90] S.F. Fennessey, R.J. Farris, Polymer 45 (2004) 4217–4225.

[91] S. Megelski, J. S. Stephens, D. B Chase, J. F. Rabolt, Micro and Nanostructured Surface Morphology on Electrospun Polymer Fibers, Macromolecules 35 (2002) 8456-8466.

[92] P. Heikkilä, A. Harlin 2008, Parameter study of electrospinning of polyamide-6, Eur. Polym. J. 44 (2008) 3067-3079.

[93] J. S. Lee, K. H. Choi, H. D. Ghim, S. S. Kim, D. H. Chun, H. Y. Kim et al., Role of molecular weight of atactic poly(vinyl alcohol) (PVA) in the structure and properties of PVA nanofabric prepared by electrospinning, J. Appl. Polym. Sci. 93(4) (2004) 1638-46.

[94] C. Wang, C. H. Hsu, J. H. Lin, Scaling laws in electrospinning of polystyrene solutions, Macromolecules 39(22) (2006) 7662–72.

[95] V. Pornsopone, P. Supaphol, R. Rangkupan, S. Tantayanon, Electrospinning of methacrylate-based copolymers: effects of solution concentration and applied electrical potential on morphological appearance of as-spun fibers, Polym. Eng. Sci. 45(8) (2005) 1073-80.

[96] L. Li, Y. L. Hsieh, Ultra-fine polyelectrolyte fibers from electrospinning of poly (acrylic acid), Polymer 46(14) (2005) 5133-9.

[97] P. Supaphol, C. Mit-Uppatham, M. Nithitanakul, Ultrafine electrospun polyamide-6 fibers: effect of emitting electrode polarity on morphology and average fiber diameter, J. Polym. Sci. B. Polym. Phys. 43(24) (2005) 3699-712.

[98] L. Brannon-Peppas, Polymers in controlled drug delivery, Med. Plast. Biomater. 4 (1997) 34-44.

[99] M.S. Romero-Cano, B. Vincent, Controlled release of 4-nitroanisole from poly (lactic acid) nanoparticles, J. Control. Release 82 (2002) 127-135.

[100] R. Langer, N.A. Peppas, Advances in biomaterials, drug delivery, and bionanotechnology, Bioeng. Food Nat. Prod. 49 (2003) 2990-3006.

[101] W. Ji, F. Yang, J. J. J. P. van den Beucken , Z. Bian , M. Fan , Z. Chen, J. A. Jansen, Fibrous scaffolds loaded with protein prepared by blend or coaxial electrospinning, Acta Biomater. 6 (2010) 4199-4207.

[102] E. R. Kenawy, F. I. Abdel-Hay, M. H. El-Newehy, G. E. Wnek, Processing of polymer nanofibers through electrospinning as drug delivery systems, Mater. Chem. Phys. 113(1) (2009) 296-302.

[103] X. Zong, K. Kwangsok, F. Dufei, R. Shaofeng, B. S. Hsiao, B. Chu, Polymer 43 (2002) 4403-4412.

[104] X. Huang, C. S. Brazel, J. Control. Release 73 (2001) 121-136.

[105] I. Moreno, V. González-González, J. Romero-García, Control release of lactate dehydrogenase encapsulated in poly (vinyl alcohol) nanofibers via electrospinning, Eur. Polym. J. 47 (2011) 1264-1272.

[106] I. C. Liao, S. Y. Chew, K.W. Leong, Aligned core–shell nanofibers delivering bioactive proteins, Nanomedicine 1(4) (2006) 465-471.

[107] H. Qi, P. Hu, J. Xu, A. Wang, Encapsulation of Drug Reservoirs in Fibers by Emulsion Electrospinning: Morphology Characterization and Preliminary Release Assessment, Biomacromolecules 7 (2006) 2327-2330.

[108] X. Xu, X. Zhuang, X. Chen, X. Wang, L. Yang, X. Jing, Preparation of Core-Sheath Composite Nanofibers by Emulsion Electrospinning, Macromol. Rapid Commun. 27 (2006) 1637-1642.

[109] A. Yoo. K. Carrageenan, micropellets production and dissolution behavior, Göttingen Cuvillier (2008) 9.

[110] K. Park, W. S. W. Shalaby, H. Par, Biodegradable Hydrogels for Drug Delivery, CRC Press (1993) 1.

[111] S. Agarwal, A. Agarwal, D. J Apple, Textbook of ophthalmology, New Delhi : Jaypee Bros. (2002) 2072.

[112] C. G. Wilson, P. J. Crowley, Controlled Release in Oral Drug Delivery, Springer (2011) 209.

[113] M. M. De Villiers, P. Aramwit, G. S. Kwon, Nanotechnology in Drug Delivery, Springer (2008) 140.

[114] C. L. He, Z. M. Huang, X. J. Han, Liu, Ling , H. S. Zhang, L. S. Chen, 2006) Coaxial Electrospun Poly(L-Lactic Acid) Ultrafine Fibers for Sustained Drug Delivery, Journal of Macromolecular Science 45B(4) (2006) 515-524.

[115] L. Yang, M. Guiping, F. Dawei, X. Juan, Z. Hongwen, N. Jun, Effects of

solution properties and electric field on the electrospinning of hyaluronic acid, Carbohyd. Polym. 83 (2011) 1011-1015.

[116] J.H. Yu, S.V. Fridrikh, G.C. Rutledge, Production of submicrometer diameter fibers by two-fluid electrospinning, Adv. Mater. 16 (2004) 1562–1566.

[117] C. K. Lee et al., The influence of added ionic salt on nanofiber uniformity for electrospinning of electrolyte polymer, Synth. Met. 154 (2005) 209-212.

[118] M. Zamani, M. Morshed, J. Varshosaz, M. Jannesari, Controlled release of metronidazole benzoate from poly e-caprolactone electrospun nanofibers for periodontal diseases, Eur. J. Pharm. Biopharm. 75 (2010) 179–185.

[119] E.L. Van, L. Grondahl, K.N. Chua, K.W. Leong, V. Nurcombe, S.M. Cool, Controlled release of heparin from poly (e-caprolactone) electrospun fibers, Biomaterials 27 (2006) 2042–2050.

[120] X.L. Xu, X.S. Chen, X.Y. Xu, T.C. Lu, X. Wang, L.X. Yang, X.B. Jing, BCNU-loaded PEG–PLLA ultrafine fibers and their in vitro antitumor activity against Glioma C6 cells, J. Control. Release 114 (2006) 307–316.

[121] M. Miyajima, A. Koshika, J. Okada, M. Ikeda, K. Nishimura, Effect of polymer crystallinity on papaverine release from poly(L-lactic acid) matrix, J. Control. Release 49 (1997) 207–215.